



# Petrogenesis of late Ediacaran volcanic rocks of the Kerdous and Tagragra d'Akka inliers (anti-atlas Morocco): Involvement of slab-failure

Olivier Blein, Thierry Baudin, Philippe Chevremont, Dominique Gasquet

## ► To cite this version:

Olivier Blein, Thierry Baudin, Philippe Chevremont, Dominique Gasquet. Petrogenesis of late Ediacaran volcanic rocks of the Kerdous and Tagragra d'Akka inliers (anti-atlas Morocco): Involvement of slab-failure. *Journal of African Earth Sciences*, 2023, 199, pp.104831. 10.1016/j.jafrearsci.2023.104831 . hal-03938018

HAL Id: hal-03938018

<https://hal.science/hal-03938018>

Submitted on 13 Jan 2023

**HAL** is a multi-disciplinary open access archive for the deposit and dissemination of scientific research documents, whether they are published or not. The documents may come from teaching and research institutions in France or abroad, or from public or private research centers.

L'archive ouverte pluridisciplinaire **HAL**, est destinée au dépôt et à la diffusion de documents scientifiques de niveau recherche, publiés ou non, émanant des établissements d'enseignement et de recherche français ou étrangers, des laboratoires publics ou privés.

# Journal Pre-proof

Petrogenesis of late Ediacaran volcanic rocks of the Kerdous and Tagragra d'Akka inliers (anti-atlas Morocco): Involvement of slab-failure

Olivier Blein, Thierry Baudin, Philippe Chevremont, Dominique Gasquet



PII: S1464-343X(23)00004-3

DOI: <https://doi.org/10.1016/j.jafrearsci.2023.104831>

Reference: AES 104831

To appear in: *Journal of African Earth Sciences*

Received Date: 28 October 2022

Revised Date: 16 December 2022

Accepted Date: 5 January 2023

Please cite this article as: Blein, O., Baudin, T., Chevremont, P., Gasquet, D., Petrogenesis of late Ediacaran volcanic rocks of the Kerdous and Tagragra d'Akka inliers (anti-atlas Morocco): Involvement of slab-failure, *Journal of African Earth Sciences* (2023), doi: <https://doi.org/10.1016/j.jafrearsci.2023.104831>.

This is a PDF file of an article that has undergone enhancements after acceptance, such as the addition of a cover page and metadata, and formatting for readability, but it is not yet the definitive version of record. This version will undergo additional copyediting, typesetting and review before it is published in its final form, but we are providing this version to give early visibility of the article. Please note that, during the production process, errors may be discovered which could affect the content, and all legal disclaimers that apply to the journal pertain.

© 2023 Published by Elsevier Ltd.

1      **Petrogenesis of late Ediacaran volcanic rocks of the Kerdous and Tagagra**

2            **d'Akka inliers (Anti-Atlas Morocco): Involvement of slab-failure**

3      Olivier BLEIN<sup>1</sup>, Thierry BAUDIN<sup>1-2</sup>, Philippe CHEVREMONT<sup>1</sup>, Dominique GASQUET<sup>3</sup>

4      <sup>1</sup> BRGM, ISTO, UMR 7327, 3 av. Claude Guillemin, BP 36009, 45060 Orléans Cédex, France,

5      [\*o.blein@brgm.fr\*](mailto:o.blein@brgm.fr)

6      ORCID : 0000-0003-3514-9641

7      <sup>2</sup> CNRS/ISTO, UMR 7327, 1A rue de la Férollerie, 45071 Orléans Cédex, France

8      <sup>3</sup> Université Savoie Mont Blanc, Laboratoire EDYTEM, UMR 5204 CNRS, Bâtiment Pole Montagne,

9      Campus Scientifique, 73376 Le Bourget du Lac, France.

10     **Keywords.** Anti-Atlas, Ediacaran, ignimbrite, silicic LIPs, slab failure.

11    **ABSTRACT**

12    Late Ediacaran rocks of the Ouarzazate Group define a thin pile of sediments and pyroclastic deposits  
 13   between the Paleoproterozoic basement and the Cambrian sedimentary cover in the southern Kerdous  
 14   and Tagagra d'Akka inliers. In the Tafeltast area, terrigenous sediments with volcano-sedimentary and  
 15   pyroclastic rocks are located in grabens controlled by syn-sedimentary normal faults. The sedimentation  
 16   is characterized by a maximum flooding outlined by the Agoujgal carbonates. In the Tagagra-n-  
 17   Daouizid, the Ouarzazate Group represents the surficial emission of rhyolitic pyroclastic flows. This  
 18   pyroclastic activity was associated with continental coarse-grained sedimentary deposits. In the  
 19   Tagagra Ouahallal, the volcanic sequence is comparable to that observed in subglacial volcanoes.  
 20   Massive ash layers, intrusive pillow lavas in waterlogged deposits, stacking of lava flows, alternation of  
 21   emerged and submerged periods under shallow water, are characteristics described in sub-glacial mafic  
 22   volcanoes.

23   According to geochemical data, volcanic rocks of the Ouarzazate Group are: (i) mafic rocks with  
 24   continental flood basalt and calc-alkaline basalt affinity; (ii) high-K calc-alkaline felsic rocks, generated  
 25   by partial melting of crustal lithologies, or by an enriched mantle with involvement of crustal component;  
 26   and (iii) intermediate to felsic slab failure rocks derived through mantle processes including melting of  
 27   mafic upper portion of the subducted slab (Hildebrand and Whalen, 2017).

28 **1. Introduction**

29 In southern Morocco, the Anti-Atlas belt is characterized by inliers of Precambrian basement  
 30 unconformably overlain by a late Ediacaran to Palaeozoic sedimentary cover (Fig. 1). This Precambrian  
 31 bedrock is composed of: (1) Paleoproterozoic metamorphosed sediments and plutonic rocks; (2)  
 32 Cryogenian oceanic volcano-sedimentary rocks affected by the Pan African tectonics; (3) Early  
 33 Ediacaran continental volcano-sedimentary rocks affected by the last Pan African tectonic events; and  
 34 (4) and Late Ediacaran voluminous pyroclastic rocks (Ouarzazate Group).

35 Geological mapping, petrographic, geochemical and geochronological studies indicate that Ediacaran  
 36 volcano-sedimentary sequences consist of basaltic to rhyolitic lavas, dacitic to rhyolitic ignimbrite and  
 37 volcaniclastic rocks of variable thickness (Choubert, 1963; Hassenforder, 1987; Ouguir et al., 1996;  
 38 Youbi, 1998; Fekkak et al., 2000, 2003; Bajja, 2001; Piqué, 2003; Thomas et al., 2002, 2004; Gasquet  
 39 et al., 2005, 2008; Walsh et al., 2012; Blein et al., 2014b; Karaoui et al., 2014, 2015; Errami et al., 2020;  
 40 Yajioui et al., 2020). These deposits formed in active tectonic settings, such as a rift or more probably  
 41 in transtensional and transpressional deformation zone (Doblas et al., 2002; Thomas et al., 2004;  
 42 Gasquet et al., 2005, 2008; Blein et al., 2014b; Errami et al. 2020). Understanding of these essential  
 43 felsic pyroclastic deposits highlights the late stage of the Pan-African orogeny.

44 Geological survey, within the framework of the Moroccan National Project of Geological Mapping  
 45 (1/50,000 scale sheet map of Sidi Bou'addi, Tamazrar, Awkarda and Tlatat Ida Gougmar), gave  
 46 opportunities to acquire new geological, geochemical, and geochronological data in the Kerdous massif  
 47 and the Tagragra d'Akka (Chalot-Prat et al., 2001; Gasquet et al., 2001; Roger et al., 2005; Chèvremont  
 48 et al., 2005). The volcanic and sedimentary deposits of the Ouarzazate Group crop out episodically  
 49 between the Paleoproterozoic poly-structured basement and the Paleozoic sedimentary cover.

50 The objectives of this publication are: (i) a better constraint of the lithological units of the western Anti-  
 51 Atlas; (ii) to present new petrographic and geochemical data on igneous rocks from the Tagragra d'Akka  
 52 and the Kerdous-Tafeltast inliers; (iii) to compare the two inliers; and (iv) to discuss the geodynamical  
 53 context at the end of the Ediacaran.

54 **2. Regional setting**

55 South of the South Atlas Fault, the Anti-Atlas belt is subdivided into three geographic domains (Fig. 1):  
 56 (i) the western Anti-Atlas characterized by Paleoproterozoic metamorphosed sediments and plutonic  
 57 rocks in the Bas Drâa, Ifni, Kerdous, Tagragra d'Akka, Tagragra de Tata, Zenaga, Iguerda, Agadir-

58 Melloul and Ighrem inliers; (ii) the central Anti-Atlas with Cryogenian island-arc – basin sequences in  
 59 the Sirwa massif and the Bou-Azer Inlier; and (iii) the eastern Anti-Atlas with thick Ediacaran volcano-  
 60 sedimentary sequences in the Saghro massif and the Ougnat inlier (Ennih and Liégeois, 2008).

61 Within the Kerdous-Tafeltast and Tagagra d'Akka inliers (Fig. 1), Precambrian rocks have been divided  
 62 in five main lithological units, corresponding to major geodynamic events: (1) Paleoproterozoic  
 63 metasedimentary schists, (2) Paleoproterozoic plutonic suites, (3) late Paleoproterozoic-  
 64 Mesoproterozoic sediments, (4) Ediacaran volcano-sedimentary and volcanic rocks, and (5) a late  
 65 Ediacaran - early Cambrian sediments.

## 66 **2.1. Paleoproterozoic rocks**

67 The Paleoproterozoic basement crops out in several inliers (Fig. 1; Ifni, Ighrem, Kerdous, Zenaga,  
 68 Tagagra d'Akka etc.), and is composed of metamorphic and magmatic rocks (Aït Malek et al., 1998;  
 69 Thomas et al., 2002; Walsh et al., 2002; Blein et al., 2022). The metamorphic rocks consist of  
 70 greenschist to amphibolite facies siliciclastic rocks and migmatites (Zenaga Group). The  
 71 metasedimentary rocks are fine-grained sandstones with interbedded volcanic layers. In the Tagagra  
 72 de Tata inlier, felsic metatuffs have been dated at  $2072 \pm 8$  Ma (Walsh et al., 2002). In the Kerdous inlier,  
 73 metamorphosed siliciclastic sediments are intruded by Rhyacian ( $2187 \pm 33$  Ma, O'Connor, 2010;  
 74  $2106 \pm 12$  Ma, Blein et al., 2022) and Orosirian granitoids (ca. 2.04-2.06 Ga, Gasquet et al., 2004;  
 75 O'Connor, 2010). According to Nd model ages (Mrini, 1993; Mortaji et al., 2000), the source of these  
 76 siliciclastic sediments is Archean.

77 Two main Orosirian plutonic events led to the intrusion of (Gasquet et al., 2008; Blein et al., 2022): (i) a  
 78 calc-alkaline suite composed of diorites, monzodiorites, granodiorites and granites originating from a  
 79 mantle source with involvement of crustal material (Azguemerzi Suite); and (ii) peraluminous granites  
 80 and leucogranites originating from a crustal source (Tazenakht Suite) into the metamorphosed  
 81 siliciclastic rocks.

## 82 **2.2. Proterozoic sediments**

83 From late Paleoproterozoic, the northern edge of the West African Craton is a passive margin which  
 84 sediments, unconformably overlying the Paleoproterozoic basement, are termed the Lkest-Taghdout  
 85 Group (Zenaga, Agadir-Melloul and Iguerda inliers; Thomas et al., 2002; Blein et al., 2013; Chèvremont

86 et al., 2013; Soulaimani et al., 2013), the Lkest Group (Kerdous inlier; BGS, 2001a, b) or the Tizi  
 87 n'Taghatine Group (central Anti-Atlas; Bouougri and Saquaque, 2004). These sediments are quartzites,  
 88 siltstones and stromatolitic carbonates, and were considered as Neoproterozoic, marking the opening  
 89 of the Bou Azer ocean (Clauer, 1976; Bouougri and Saquaque, 2004; Thomas et al., 2004). However,  
 90 this assumption is now questioned since detrital zircon ages of these sediments point to a maximum  
 91 age of deposition around 1.8 to 1.7 Ga (Abati et al., 2010; Soulaimani et al., 2019). This age estimate is  
 92 corroborated by age determinations on baddeleyite and zircon ages of crosscutting mafic sills and dykes  
 93 (ca. 1.71 Ga: Ikenne et al., 2017, Youbi et al., 2013; ca. 1.63 Ga: Kouyate et al., 2013, Aït Lahna et al.,  
 94 2020), and on pegmatites (ca. 1.76 Ga: Gasquet et al., 2004).

### 95 **2.3. Ediacaran sedimentary and magmatic events**

96 During Lower Ediacaran (before 580 Ma), volcano-sedimentary rocks are known as the Saghro Group  
 97 (central and Eastern Anti-Atlas), the Anezi series (western Anti-Atlas), the Tiddiline Group (central Anti-  
 98 Atlas), and the Bou Salda Group (eastern Anti-Atlas). During Upper Ediacaran (after 580 Ma), volcano-  
 99 sedimentary rocks associated with high-level granites are known as the Ouarzazate Group throughout  
 100 the entire Anti-Atlas.

101 Extending from the Sirwa to Ougnat massifs, the Saghro Group is composed of ca. 6000 m thick of  
 102 deformed turbidites; the sedimentary cycles tend to be composed of shales, siltstones and sandstones  
 103 that coarse upward, with carbonates (Thomas et al., 2002; Fekkak et al., 2003; Eddif et al. 2007; Pelleter  
 104 et al., 2007; Michard et al., 2017). Recent U-Pb datations on detrital zircons characterized a maximum  
 105 depositional age of  $604 \pm 5$  Ma (Errami et al. 2020).

106 Volcano-sedimentary rocks of the Anezi-Tiddiline-Bou Salda Group were deposited in subsident narrow  
 107 grabens lined to a transtensive context (Thomas et al., 2004; Blein et al., 2014a). Felsic ignimbrites of  
 108 the Bou Salda and Tiddiline groups have given U-Pb zircons ages of ca. 607–605 Ma (Thomas et al.,  
 109 2002; Blein et al., 2014a). These volcano-sedimentary rocks deposits have been deformed between  
 110 these last ages and ca. 580 Ma, and unconformably overlain by pyroclastic flows of the Ouarzazate  
 111 Group (Blein et al., 2014a).

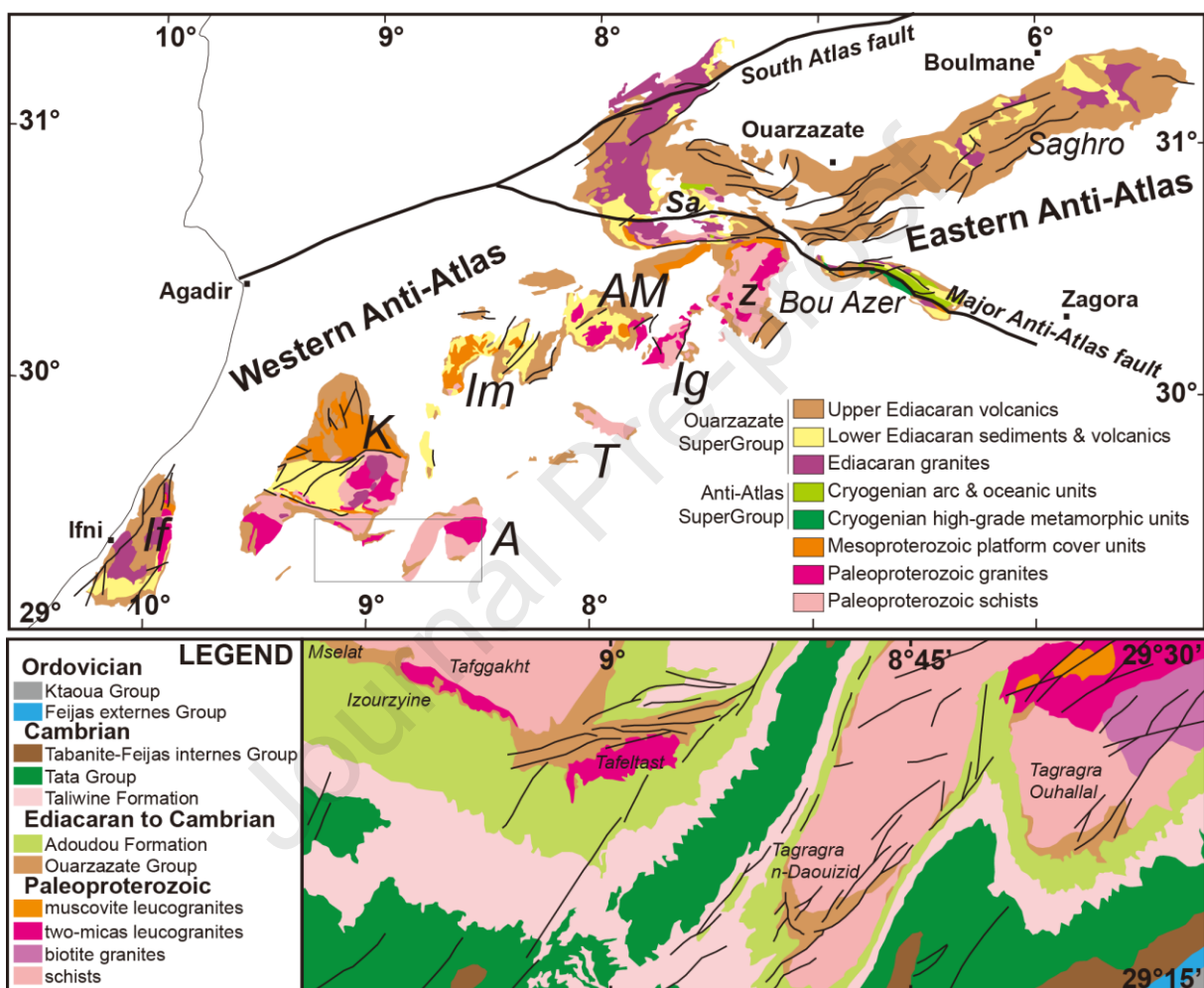
112 Upper Ediacaran rocks (post 580 Ma) comprise sedimentary, volcano-sedimentary, pyroclastic and  
 113 volcanic rocks, with locally sub-volcanic granitic rocks. Pyroclastic and volcanic rocks have high-K calc-  
 114 alkaline to shoshonitic affinities, and plutonic rocks are essentially I- and S-type granitoids, with local A-

115 type granitoids intrusions (Thomas et al., 2002; El Baghdadi et al., 2003; Gasquet et al., 2005; Errami  
 116 et al., 2009; Toummite et al., 2012; Walsh et al., 2012; Blein et al., 2014b; Baidada et al., 2017; Belkacim  
 117 et al., 2017). U-Pb zircon ages for these intrusions range between ca. 575–542 Ma (Hawkins et al.,  
 118 2001; Cheillett et al., 2002; Walsh et al., 2002; Gasquet et al., 2005; Blein et al., 2014a, b; Karaoui et  
 119 al., 2015). In the Central Anti-Atlas, the large variations in the thickness of the Ouarzazate Group are  
 120 controlled by a pronounced paleo-relief. These volcano-sedimentary rocks are locally affected by syn-  
 121 sedimentary deformation (SE striking folding and NE-SW faulting; Blein et al., 2014b),  
 122 In the Central Anti-Atlas, the important thickness variations of the volcaniclastic Ouarzazate deposits  
 123 are controlled, at the first order, by an accented horst and graben paleogeography (Blein et al., 2014b).  
 124 Moreover, the successive volcaniclastic deposits are also linked to a syn-sedimentary tectonic event  
 125 such as NW-SE striking folding and NE-SW faulting (Blein et al., 2014b), suggesting contemporaneous  
 126 compressive and extensive zones in a transtensional regional context.  
 127 Two main geodynamic contexts have been proposed for the magmatism of the Ouarzazate Group: (i)  
 128 subduction related (Bajja, 1998; El Baghdadi et al., 2003; Benziane, 2007; Walsh et al., 2012; Hefferan  
 129 et al., 2014); or (ii) post-collisional with respect to the Pan-African arc-continental main collisional event  
 130 (Thomas et al., 2002; Gasquet et al., 2005, 2008; Toummite et al., 2012). Blein et al. (2014a, b) have  
 131 proposed an origin linked to a slab breakoff that occurred between ca. 580–575 Ma. The subsequent  
 132 magmatism following slab breakoff is felsic, and results from partial melting of continental crust.

#### 133 **2.4. Late Ediacaran to Cambrian sedimentation**

134 The Late Ediacaran volcanic and volcano-sedimentary rocks of the Ouarzazate Group are  
 135 unconformably overlain by a thick carbonate to clastic sedimentary cover comprising from bottom to top:  
 136 (i) the transgressive late Ediacaran to early Cambrian Taroudannt Group, (ii) the Cambrian Tata Group,  
 137 and (iii) the Cambrian to Ordovician transgressive groups of internal Feijas, Tabanite, external Feijas,  
 138 and Ktaoua. The Taroudannt Group is composed by the carbonate-dominated Adoudou Formation and  
 139 the terrigenous-carbonate-dominated Taliwine Formation, which is dominantly carbonate westward and  
 140 exclusively terrigenous further east (Choubert, 1952, 1953a, b). Carbonates of the Adoudou Formation  
 141 have microbial origin structures, and characterize a regional subsidence context responsible for the  
 142 progressive flooding of the Anti-Atlas, from West to East (Boudda et al., 1979; Geyer, 1990; Bensaou  
 143 and Hamoumi, 2001; Alvaro et al., 2005, 2014). Locally, volcanic lavas occur interbedded within

144 sediments of the uppermost part of the Adoudou Formation. This context is interpreted as continental  
 145 rifting (Piqué et al., 1999; Bensaou and Hamoumi, 2001, 2003; Soulaimani et al., 2003).  
 146 U/Pb age determinations from the Boho volcano ( $529 \pm 3$  Ma; Ducrot and Lancelot, 1977) and from the  
 147 Aghbar trachyte sill ( $531 \pm 5$  Ma; Gasquet et al., 2005) suggests a Cambrian age for the Adoudou  
 148 Formation, in which they are interlayered. Recently, an older U-Pb late Ediacaran age ( $542 \pm 5$  Ma; Blein  
 149 et al., 2014b) has been obtained on volcanic breccia at the base of the Adoudou Formation.



150  
 151 **Figure 1:** Precambrian geology of the Anti-Atlas inliers (modified from Hollard et al. 1985, Walsh et al.  
 152 2002, and Gasquet et al. 2008). A: Tagagra d'Akka; AM: Agadir-Melloul; BD: Bas Drâa; If: Ifni; Ig:  
 153 Iguerda; Im: Igherm; K: Kerdous; Sa: Sirwa; T: Tagagra de Tata).

154

155 **3. Field relationships and petrography**

156 Geological mapping, carried out within the National Geological Mapping Plan of Morocco, allows to  
 157 establish a new lithostratigraphic chart of the Proterozoic rocks (Thomas et al., 2004). In discontinuity  
 158 with the Anti-Atlas Supergroup (800-680 Ma), the Ouarzazate Supergroup (615-542 Ma) is  
 159 characterized by continental deposits and post-orogenic magmatism accumulates in a graben system.  
 160 The Ouarzazate Group defined on the present Awkarda map sheet, as well as on the eastern sheets of  
 161 Sidi Bou'addi and Tamazrar is the upper part of the Ouarzazate Supergroup defined by Thomas et al.  
 162 (2004). In the entire Anti-Atlas, the deposits of the Ouarzazate Group are included in an age range  
 163 between ca. 575–542 Ma (Hawkins et al., 2001; Cheillett et al., 2002; Walsh et al., 2002; Gasquet et  
 164 al., 2005; Blein et al., 2014a, b; Karaoui et al., 2015).

165 The Ouarzazate Group is mainly composed of fluvial-lacustrine deposits accumulated in small basins  
 166 bordered by high levels (Tagagra Ouhallal, Tagagra-n-Daouizid, Tafeltast, and south of Zawyat-n-  
 167 Dougadir; Fig. 1). This sedimentation is contemporary with volcanic and pyroclastic flows. Volcanic and  
 168 sedimentary deposits accumulate on the margin of narrow grabens, and exhibit high lateral and upward  
 169 variations. Volcanic and sedimentary rocks are sub-conformably overlain by the late Ediacaran  
 170 sediments of the Adoudou Formation.

171 **3.1. Kerdous inlier**

172 In the Tafeltast area, the Ouarzazate Group is composed of sediments with few volcano-sedimentary  
 173 rocks, and high vertical and lateral variations (Figs. 2A and 3), with a thickness ranging between 0 to  
 174 250 m. Volcano-sedimentary deposits are located in a NE striking narrow half-graben controlled by syn-  
 175 sedimentary normal faults. The NW limit is a SE dipping normal fault, and the SE limit is the top of a  
 176 tilted block. The Ouarzazate Group is conformably overlain by late Ediacaran marine sediments  
 177 (Adoudou Formation), which are contemporaneous with a less and less active syn-sedimentary  
 178 extensive tectonism.

179 The Ouarzazate Group sediments were deposited in a fluvial-lacustrine setting in a tectonic and  
 180 magmatic active system. The fluvial-lacustrine sediments unconformably overlie the Paleoproterozoic  
 181 basement with a basal sedimentary breccia. This breccia rapidly evolves laterally and upward to finer  
 182 silts (the lower silts facies, Fig. 3). The vertical aggradation of the rapid limit between breccia and  
 183 siltstone indicates a progressive deepening of the graben during the Upper Ediacaran. In the middle of  
 184 the sedimentary pile, breccia and silts are overlain by a carbonate sedimentation, the Agoujgal  
 185 carbonates (a carbonate key bed), which marks a maximum flooding (Figs. 2A and 3).

186 This lacustrine sedimentation presents therefore a complete transgressive and regressive cycle. The  
 187 basal and lateral breccia reaches one to 20 m thickness and includes heterometric blocks of  
 188 Paleoproterozoic basement: schist, quartzite, gabbro, dolerite and granite. The petrography of the  
 189 blocks reflects the lithology of the closer Paleoproterozoic basement, suggesting a very limited transport  
 190 of sediments. Two types of breccia may be mapped: breccia with schists or granite dominant blocks.

191 The basal breccia with Paleoproterozoic schist blocks outlines the northern border of the Ediacaran  
 192 graben (Fig. 2A). The clasts, angular and unclassified, suggest a limited transport. Volcanic lenses  
 193 stratified in these breccias outline the occurrence of a contemporaneous volcanism. The  
 194 Paleoproterozoic basement is often affected by metric faulting zones with tectonic breccias. The  
 195 progressive change from tectonic to sedimentary breccias suggests that the first feeds the second. Basal  
 196 breccias are related to the development of normal faults which are at the origin of the Ediacaran grabens.

197 The basal breccia with Paleoproterozoic granite blocks outlines the southern limit of the Upper  
 198 Ediacaran graben (Fig. 2A). Breccias result from reworking of a granitic arena on a slight slope dipping  
 199 to the north, and are pinching out to the south. Then, the Paleoproterozoic basement is overlain by the  
 200 last volcanic flows of the Ouarzazate Group, or by the sediments of the Adoudou Formation. This setting  
 201 suggests the existence of paleo-relief with horst structure composed of Paleoproterozoic basement to  
 202 the south.

203 The Agoujgal carbonates, representing a maximum flooding surface, are a key bed in the Ediacaran  
 204 sedimentary sequence of the Tafeltast area. The number and thickness of carbonate levels increase  
 205 from the southern border to the middle of the basin. In the central part of the basin, six carbonate levels  
 206 with a decreasing thickness from 25 to 3 meters have been observed. The basal carbonate level crops  
 207 out from the southern border to the center of the basin. The Agoujgal Formation is characterized by the  
 208 following stratigraphic facies: i) the basal calcareous of Agoujgal; ii) alternating between carbonate,  
 209 siltstone and volcanic rock; and iii) alternating between carbonate, conglomerate and volcanic rock. The  
 210 two latter associations are contemporaneous. They overlie the basal carbonate level. The Agoujgal  
 211 carbonates are composed of light dolosparite stratified in decimetric beds. This lithofacies is  
 212 characterized by an algo-bacterial lamination, that is often silicified, and quartz-rich fine layers. Few  
 213 rhyolitic lenses are interbedded in these carbonates.

214 Alternating carbonates, siltstones and volcanic rocks (metric to decametric thickness) mark the  
 215 beginning of the regressive interval which results in a decreasing number, extension and thickness of  
 216 the carbonate levels in favor of the silty terrigenous sedimentation. Towards the top, carbonates and  
 217 volcanic rocks tend to disappear, giving way to the purely terrigenous sedimentation of the upper  
 218 siltstones.

219 On the southern edge of the graben, siltstones are laterally replaced by conglomeratic deposits, which  
 220 prograde and end up the upper conglomerates. Interlayered and lenticular volcanic emissions occur as  
 221 lava flows, ignimbrites or block lava flows.

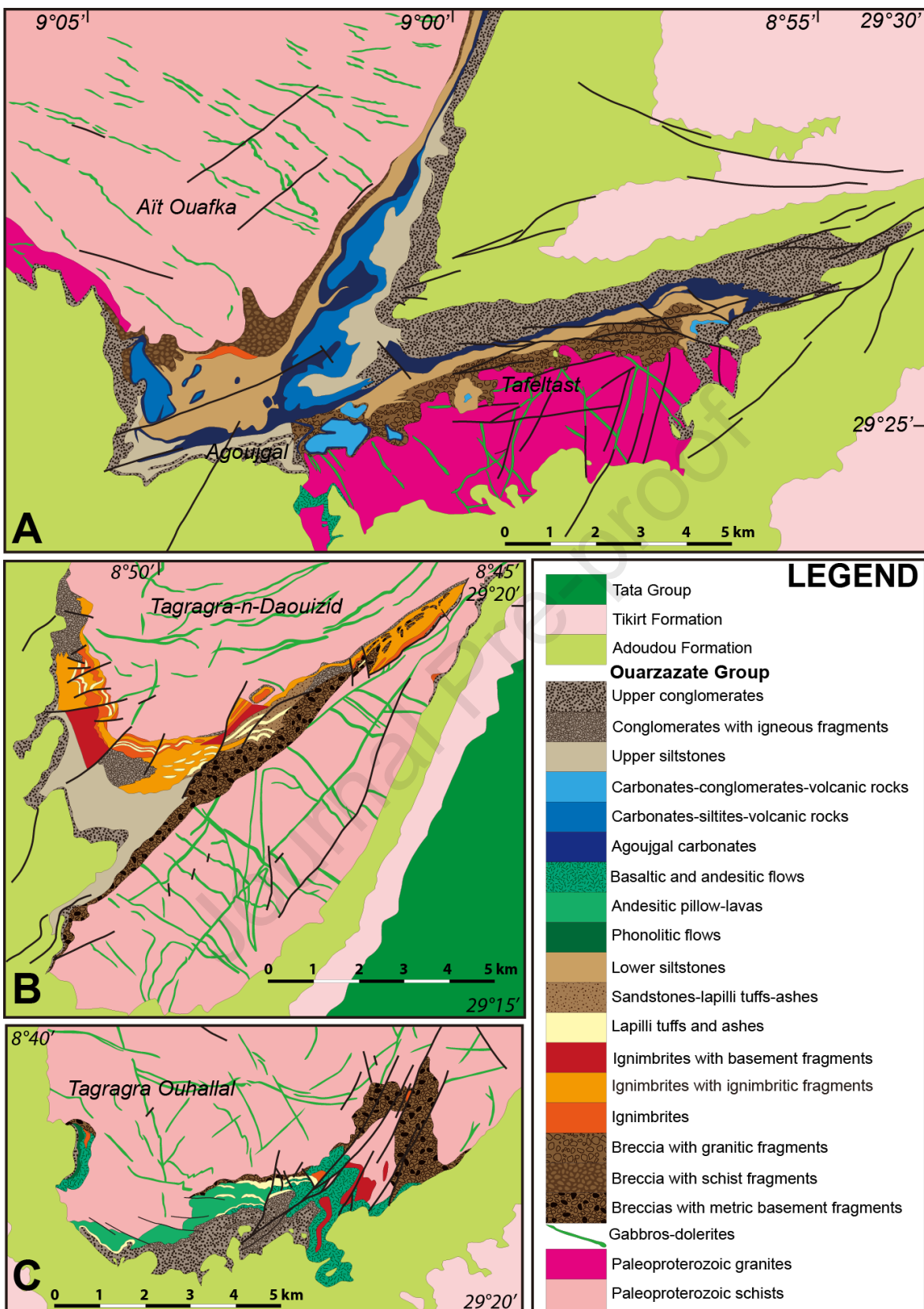
222 Volcanic deposits are localized on the emerging borders of the basin, and in lenses interbedded in the  
 223 sediments of the Agoujgal Formation (Figs. 2A and 3). Volcanic rocks are basaltic lavas flows or rhyolitic  
 224 pyroclastic deposits, with limited geographic extension. All the emission centers rest on the  
 225 Paleoproterozoic granitic basement. Volcanic deposits are overlain by the last sequence of the upper  
 226 conglomerates or by the basal deposits of the Adoudou Formation. The volcanic activity was locally still  
 227 active until the basal deposits of the Adoudou Formation. This mafic volcanism is latter than one which  
 228 outcrops in the Tagragra Ouhallal area localised than SE. Basalts have microlitic to intersertal, more or

229 less porphyritic textures with the following mineralogy: feldspar, oxides, apatite, sericite, chlorite, calcite,  
230 hydroxides with sometimes the asserted presence of altered olivine.

231 Rhyolitic pyroclastic flows form an east-west trending crest that joins the north of Mselat to the peaks  
232 east of Tafggakht. They are marked in the landscape by a multi-decameter alternation of white and dark  
233 colors despite their comparable chemistry. The dark color could be the result of a higher proportion of  
234 glass in the matrix. Pyroclastic flows are locally separated by lapilli tuffs of multi-decimetre thickness.  
235 North of Mselat, the first volcanic level is a dark brecciated glass-clastic tuff that flows over basal  
236 breccias with dominant granitic elements about 15 metres thick; the latter resting on Paleoproterozoic  
237 schists. To the east and south of Tafggakht, the Paleoproterozoic granite is directly overlain by an  
238 ignimbritic bedded rhyolite. These rhyolitic deposits are almost entirely covered by the upper  
239 conglomerates. These conglomerates are characterized by - locally metric - rhyolitic blocks.

240 The second rhyolitic flow to the NE of Mselat, about 50 m thick, was U/Pb dated on zircon by the  
241 SHRIMP method and provided an age of  $561 \pm 6$  Ma (Chèvremont et al., 2005). This porphyritic rhyolite  
242 shows a fluid glass-clastic texture with phenocrysts of feldspar, quartz, oxides, sericite, pumpellyite, and  
243 micro-lapilli.

244 Andesitic to dacitic pyroclastic flows cap the tops of the Izourzine cliff and are clearly visible, with their  
245 dark color contrasting with the light granite. They lie directly on the Paleoproterozoic granite and often  
246 show flat- or cross-bedded ash cloud surge figures that outline gully channels and ash levels. This type  
247 of structure is reminiscent of ash cloud deposits. These deposits are directly surmounted by the upper  
248 conglomerates with rolled pebbles, and without volcanic elements.



249

250 **Figure 2:** Simplified geologic maps: **A.** the Kerdous inlier (Baudin et al., 2005; Hassenforder et al.,  
 251 2001); **B.** the Tagagra-n-Daouzid area (Hassenforder et al., 2001); and **C.** the Tagagra Ouhallal  
 252 area (Roger et al., 2001).

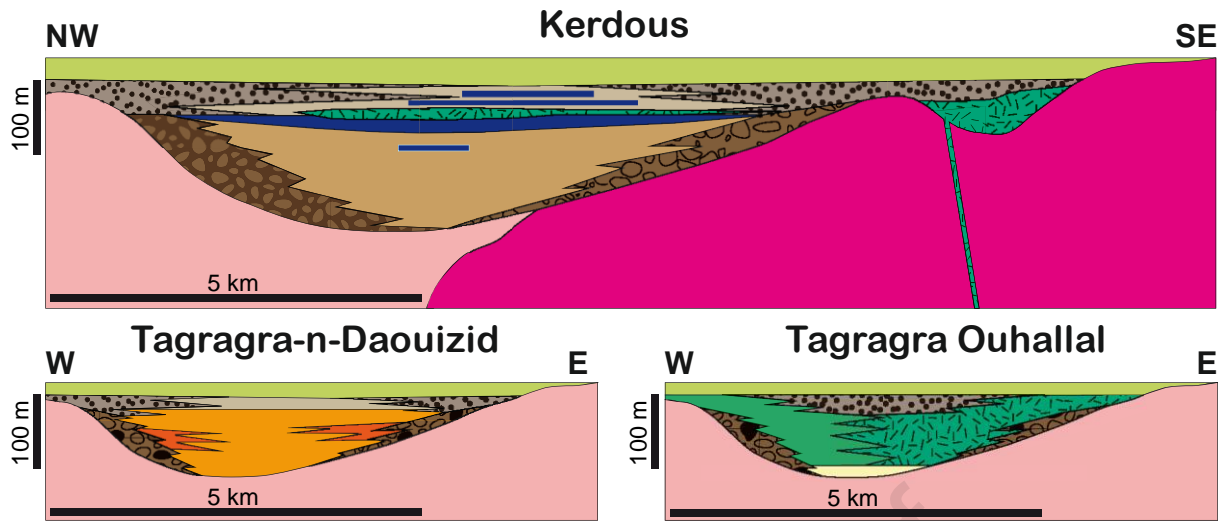


**Figure 3:** Schematic distribution of the different lithostratigraphic units. Symbols as in Fig. 2.

### 255 **3.2. Tagragra-n-Daouizid area**

256 In the Tagragra-n-Daouizid area, the Ouarzazate Group is composed of conglomerates, volcano-  
 257 sedimentary rocks with pyroclastic rocks, and high vertical and lateral variations (Fig. 2B), with a  
 258 thickness ranging between 0 to 100 m. The basal chaotic breccias are characterized by heterometric  
 259 and heterolithic blocks, essentially substrate-derived rocks such as schist, granite, quartzite, dolerite  
 260 and gabbro (Figs. 2B and 3). The lithology of the clasts reflects the lithology of the local basement, the  
 261 distance of transport of clasts was limited. The breccias are observed at the base of clast-rich ignimbrites  
 262 which beginning the volcanic sequence. These breccias are not restricted to the base of the volcanic  
 263 sequence, they also crop out stratified in the middle and at the top of the volcanic sequence. They are  
 264 related to fault-controlled scarps which were activated prior to volcanic eruptions. The regular  
 265 occurrences of these chaotic breccias suggest that the faults were still active during all the volcanic  
 266 activity.

267 Sandstones stratified with lapilli tuffs and ashes are well established in the center of the volcano-  
 268 sedimentary sequence. Sandstones are light, fine to middle grained, and quartz-feldspathic in  
 269 composition. Stratified in beds, they are covered without transition with a few meter thick of chaotic  
 270 breccias observed at the top of an ignimbritic unit, and alternate regularly with well stratified tuffs. These  
 271 sandstones are river deposits in shallow water. The rapid change between breccias and sandstones,  
 272 suggest that the formation of the breccias is independent from the river system which control the  
 273 sandstone deposits.

274 On top, the Ouarzazate Group is characterized by pelitic facies such as silts. These silts are interbedded  
 275 with micro-conglomeratic sandstones which are more abundant at the top of the sedimentary sequence  
 276 (Figs. 2B and 3). These silts overlie conformably ignimbrites, conglomerates and breccias, and  
 277 constitute a lenticular lens in the central part of the grabens. Silts are certainly lake deposits, and mark  
 278 the end of pyroclastic density currents such as ignimbrites. The deposits herald the end of the maximum  
 279 basement deformation. However, ash fall deposits and coarse grained sandstones occur locally.

280 The youngest deposits of the Ouarzazate Group are polygenic conglomerates and coarse-grained  
 281 sandstones, with a large geographic extension overlying previous sedimentary and pyroclastic rocks  
 282 and the Paleoproterozoic rocks.

283 Ediacaran volcanism is characterized by numerous pyroclastic flows. Massive lapilli tuffs with basement  
 284 blocks overlie the Paleoproterozoic basement, chaotic breccias or basal conglomerates. Basement  
 285 blocks are derived from collapse or erosion of the eruption conduit or substrate by the density current.  
 286 These massive lapilli tuffs are non-welded, with little sub-rounded blocks which do not exceed one  
 287 centimetre in size. This lithofacies lacks internal stratification and comprises pumice, lithic lapilli, and  
 288 crustal fragments with a matrix of vitric ashes with crystals clasts. The thickness of volcanic deposits is  
 289 variable (a few m to 30 m maximum).

290 Massive homogenous welded pyroclastic tuffs cover the massive lapilli tuffs with basement blocks. This  
 291 ignimbrite forms massive, lenticular, 5 to 10 m thick layers, with a prismatic flow, often associated with  
 292 a planar flow. They are interbedded with inframetric layers of lapilli and ash tuffs or embedded within  
 293 thicker deposits of block ignimbrites. These ignimbrites have a vitroclastic texture, mostly unwelded and  
 294 uncompacted, with 40% splinters and pumice fragments in an ashy matrix. Some horizons have a  
 295 welded and hot compacted eutaxitic texture including a significant proportion of flames or compacted  
 296 pumice fragments. The lack of basement xenoliths and the great homogeneity of the material explain  
 297 the very frequent prismation of the deposits. The low frequency of welded tuffs means that the  
 298 pyroclastic flows have a relatively moderate temperature at the time of flow immobilization.

299 Ignimbrites may contain 20 to 50% of angular blocks of massive ignimbrite of very variable size. The  
 300 embedded blocks come from the pulverization of the older ignimbritic levels. The small width and  
 301 considerable number of interlocking channels suggest the successive and extremely rapid emission of  
 302 pyroclastic flows involving small volumes of magma.

303 Numerous fallout deposits, such as lapilli tuffs or ashes, are associated with the co-ignimbrite ash flow.  
 304 They are generally black, green or purplish grey rocks, and are fine- to medium-grained, relatively  
 305 homogeneous because they are always well sorted and locally with visible normal grading. They contain  
 306 40-50% volcanic fragments (crystal clasts; shredded pumice fragments), and angular xenoliths of  
 307 Paleoproterozoic basement, all in a matrix of very fine, siliceous ashes.

### 308 **3.3. Tagragra Ouhallal area**

309 In the Tagragra Ouhallal area, the Ouarzazate Group outcrops locally between the Paleoproterozoic  
 310 rocks and the late Ediacaran – Cambrian sediments, with a thickness ranging between 0 to 100 m (Figs.  
 311 2C and 3).

312 The volcanic sequence, highly diversified, consists of a succession of massive flows or pillow basalts of  
 313 alkaline mafic lava, and lapilli tuffs and ashes, all locally preceded by deposits of dacitic to rhyolitic  
 314 ignimbrites. All eruptions are continental and lenticular in nature. The sedimentary deposits consist of  
 315 accumulations of breccia with basement fragments, which are interbedded with conglomerate and  
 316 sandstone at the end of the volcanic sequence. The internal organization of the volcanic succession is  
 317 quite simple although it is different from east to west.

318 To the east, lava flows overlain unconformably the basement, breccias, and ignimbrites. These flows  
 319 may be overlain by breccia. Flows are massive, and interstratified with lapilli tuffs and ashes. Lavas are  
 320 porphyritic, and or microlitic and fluidal, with plagioclase and clinopyroxene and olivine.

321 In the western part, tubular and pillow lavas make up the bulk of the volcanic sequence. They cover  
 322 either the basement, basement breccia, or massive non-layered cinerites. The first pillow lavas are  
 323 secant and intrusive in finely layered lapilli tuffs and ashes. Above, pillows and tubes form extrusive  
 324 lenticular units interlayered with pyroclastic breccias, hyaloclastites and finely layered tuffs. These lavas  
 325 were deposited under water. They are covered by breccia with basement fragments.

#### 326 **4. Geochemistry**

327 Whole-rock major and trace elements were analysed by ICP-AES and ICP-MS (CRPG-CNRS, Nancy),  
 328 respectively (Tables S1, S2, and S3). Sample preparation, analytical conditions and limits of detection  
 329 are detailed in Carignan et al. (2001).

##### 330 **4.1. Kerdous inlier**

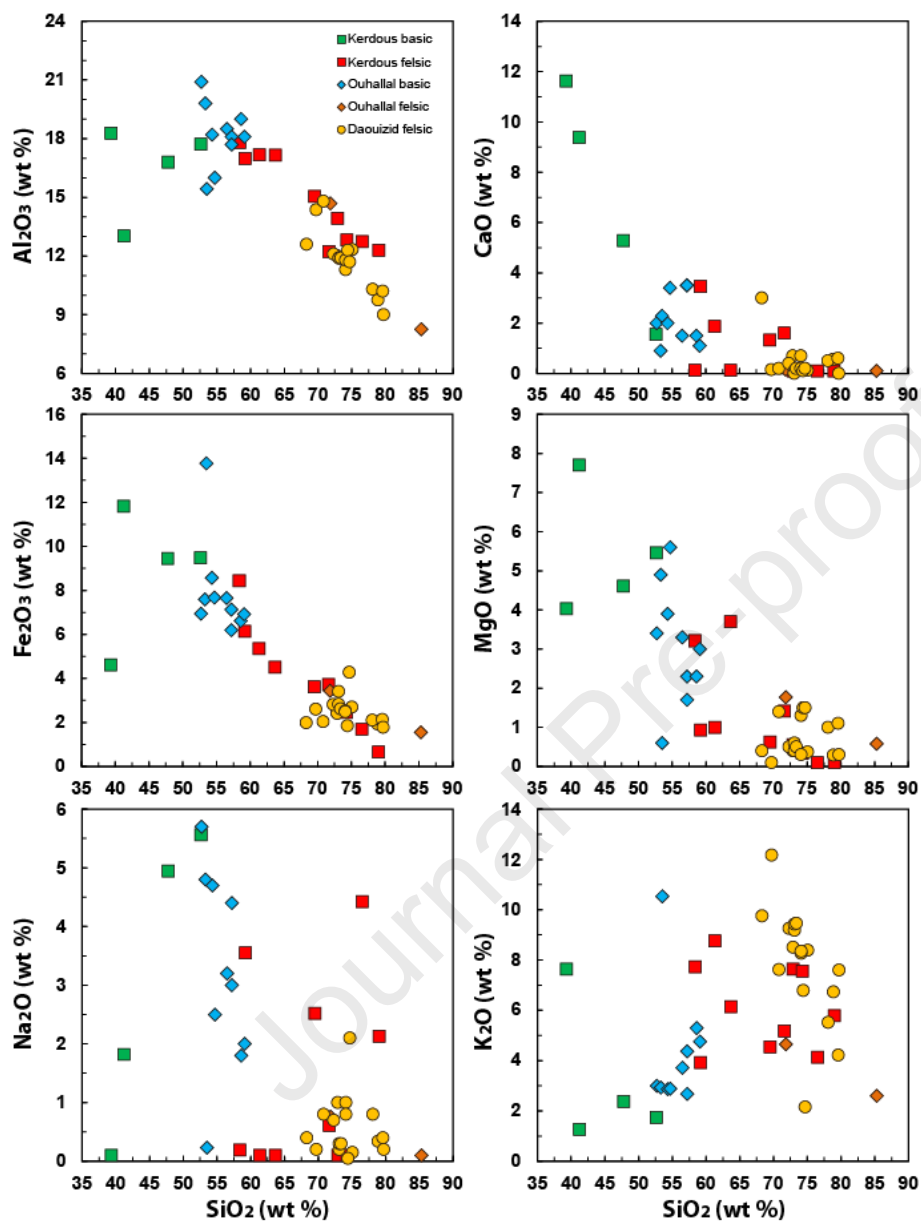
331 Four lavas are mafic in compositions ( $\text{SiO}_2=39.3\text{-}52.6 \text{ wt\%}$ ), with high  $\text{Al}_2\text{O}_3$  (13.0-18.3 wt%) and  $\text{TiO}_2$   
 332 contents (1.48-1.82 wt%), and low to high  $\text{Fe}_2\text{O}_3$  (4.6-11.8 wt%),  $\text{MgO}$  (4.0-7.7 wt%),  $\text{CaO}$  (1.6-  
 333 11.6 wt%),  $\text{Na}_2\text{O}$  (0.1-5.6 wt%), and  $\text{K}_2\text{O}$  contents (1.3-7.6 wt%; Fig. 4). Such variations on major  
 334 elements are explained by a strong loss in ignition, which is generally higher than 3.5 wt%.

335 Basaltic flows display REE patterns with fractionated LREE ( $2.1 < [\text{La}/\text{Sm}]_n < 4.3$ ), and slight or significant  
 336 fractionation of HREE (Fig. 5A). The two basalts samples with the lower concentrations in LREE have  
 337  $[\text{Gd}/\text{Yb}]_n$  ratios lower than 1.6. In contrast, the two other ones have fractionated HREE with  $[\text{Tb}/\text{Yb}]_n$   
 338 ratios higher than 2.6. Normalized to Primitive Mantle values, their patterns display negative anomalies  
 339 in Ta, Nb and Ti (Fig. 6A).

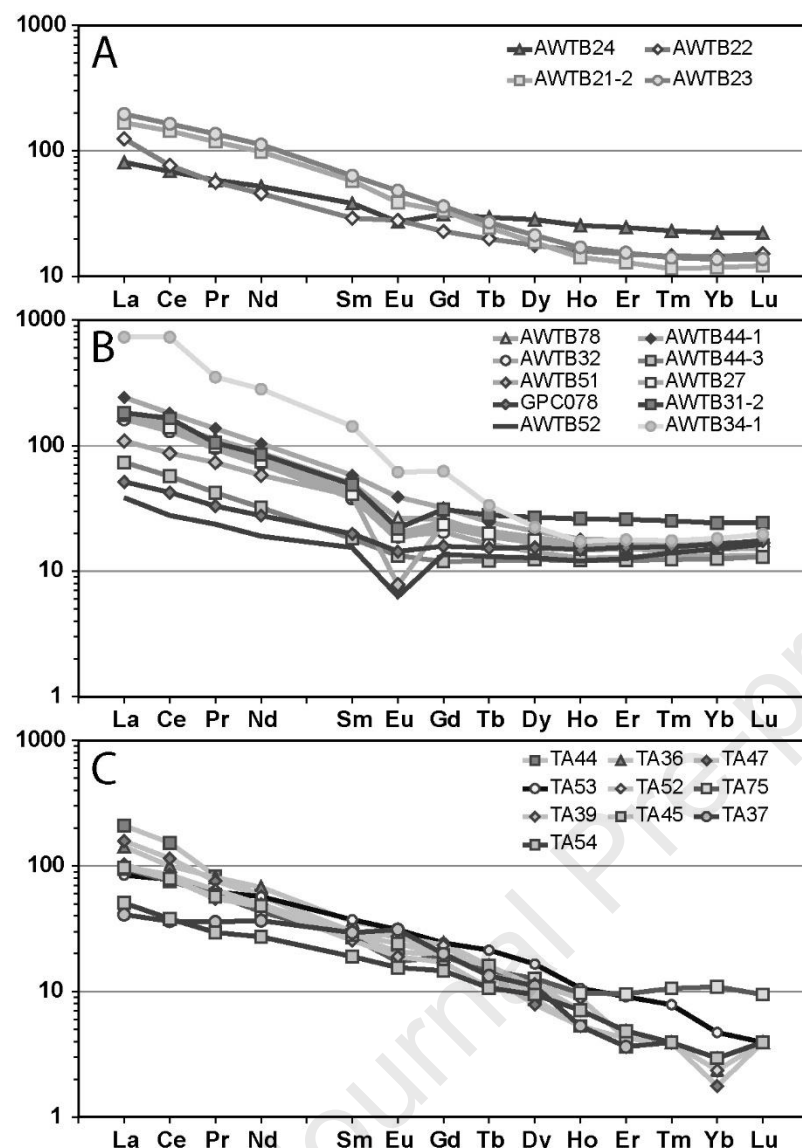
340 Three samples (AWTB27, AWTB78, and AWTB44-1) have andesitic composition ( $\text{SiO}_2=58.4\text{-}61.3 \text{ wt\%}$ ), with high  $\text{Al}_2\text{O}_3$  (17.0-17.8 wt%), and  $\text{K}_2\text{O}$  contents (3.9-8.8 wt%), low to high  $\text{Na}_2\text{O}$  contents  
 341 (0.1-3.6 wt.%), moderate  $\text{Fe}_2\text{O}_3$  (5.4-8.4 wt%), and low  $\text{MgO}$  (0.9-3.2 wt%),  $\text{CaO}$  (0.1-3.5 wt%) and  $\text{TiO}_2$   
 342 contents (0.52-0.76 wt%; Fig. 4). These lavas are peraluminous with A/CNK ratio in the range 1.04-  
 343 2.00, and show dominantly alkali, and magnesian to ferroan affinities (Fig. 7).

344 Intermediate lavas display REE patterns similar to basaltic lavas, with fractionated LREE  
 345 ( $3.5 < [\text{La}/\text{Sm}]_n < 4.3$ ), slightly fractionated HREE ( $1.5 < [\text{Gd}/\text{Yb}]_n < 1.9$ ; Fig. 5B), and moderate negative Eu  
 346 anomalies ( $0.6 < \text{Eu}/\text{Eu}^* < 0.9$ ; Fig. 5B). The lack of significant HREE fractionation suggests that parent

348 liquids have been produced out of the garnet stability field. Intermediate lavas display systematic and  
 349 high Ta, Nb and Ti negative anomalies relative to REE (Fig. 6B).

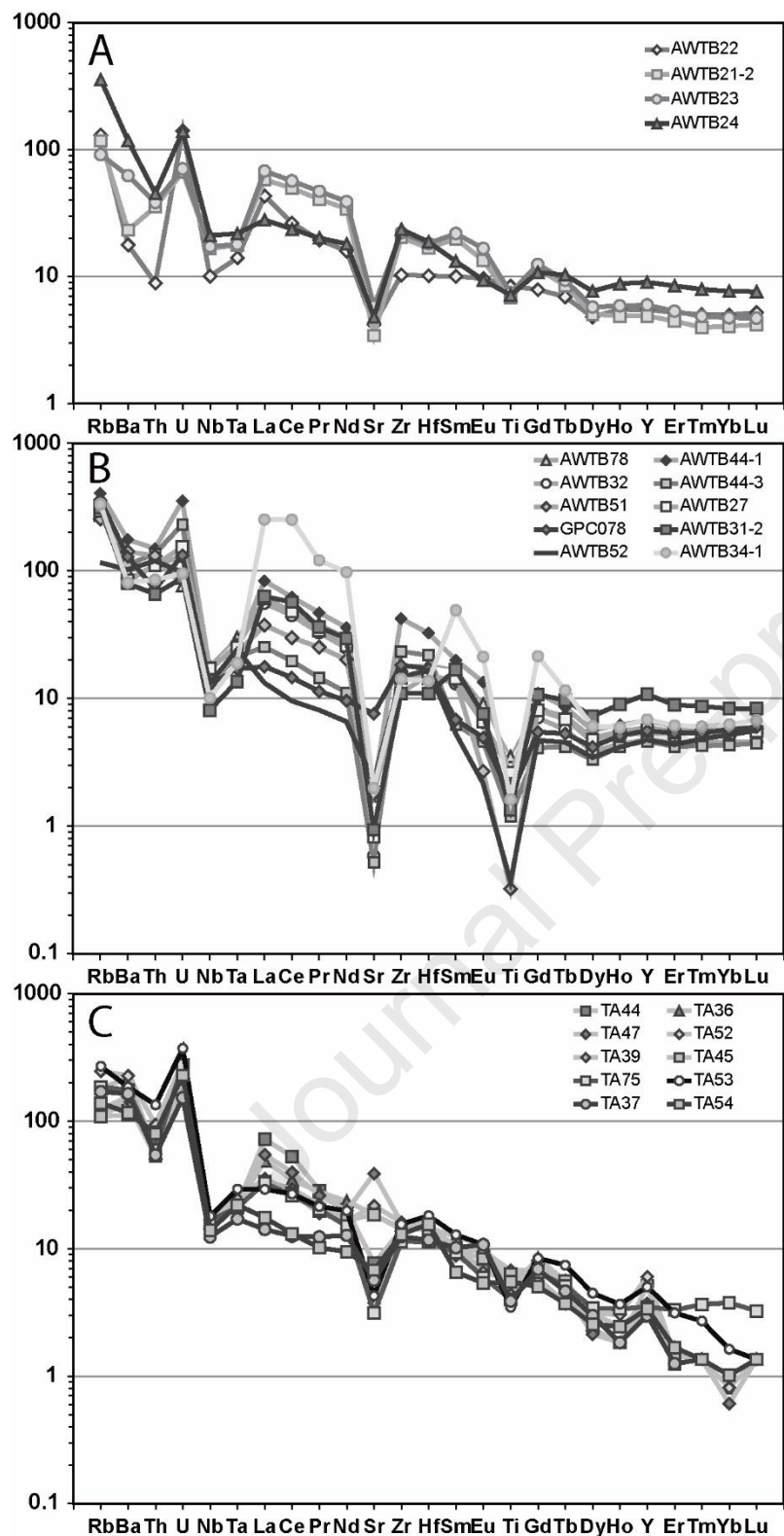


350  
 351 **Figure 4:** Harker diagrams for volcanic rocks from the Ouarzazate Group.  
 352



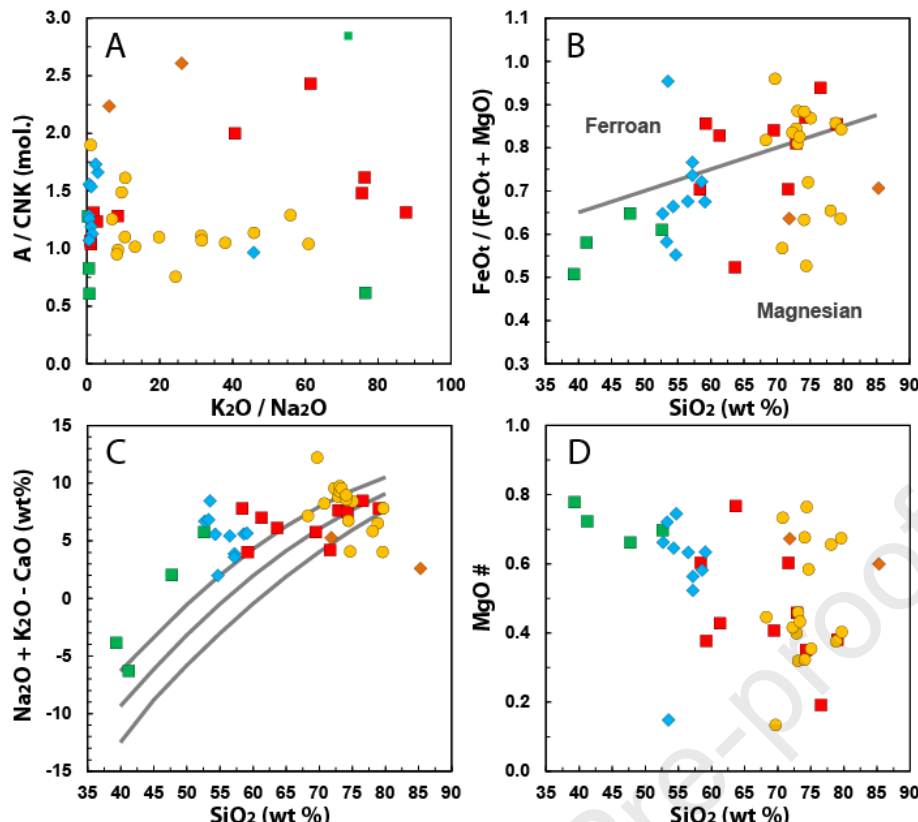
353  
354  
355  
356

**Figure 5:** Chondrite normalized rare earth element diagram of volcanic rocks from the Kerdous inlier and the Tagragra Ouhallal area. **A.** Kerdous basalts & rhyolites; **B.** Kerdous intermediate and felsic volcanic rocks; **C.** Tagragra Ouhallal samples. Normalization according to Sun and McDonough, 1989.



357

358 **Figure 6:** Primitive Mantle normalized multi-element diagram of volcanic rocks from the Kerdous inlier  
 359 and the Tagragra Ouhallal area. **A.** Kerdous basalts & rhyolites; **B.** Kerdous intermediate and felsic  
 360 volcanic rocks; **C.** Tagragra Ouhallal samples. Normalization according to Sun and McDonough, 1989.



361

362 **Figure 7:** Major-element geochemistry of the Ouarzazate Group volcanic rocks. **A.** K<sub>2</sub>O/Na<sub>2</sub>O vs.  
363 A/CNK; **B.** SiO<sub>2</sub> vs. FeO<sup>t</sup>/(FeOt+MgO); **C.** SiO<sub>2</sub> vs. MALI index ([Na<sub>2</sub>O+K<sub>2</sub>O]-CaO) diagram of Frost et  
364 al. (2001); **D.** SiO<sub>2</sub> vs. Mg#. Symbols as in Fig. 3.

365 Few samples have dacitic to rhyolitic composition (SiO<sub>2</sub>=63.7-79.0 wt%), with high Al<sub>2</sub>O<sub>3</sub> (12.2-  
366 17.2 wt%), and K<sub>2</sub>O contents (4.1-7.6 wt%), low to high Na<sub>2</sub>O contents (0.1-4.4 wt%), and low Fe<sub>2</sub>O<sub>3</sub>  
367 (0.7-4.5 wt%), MgO (0.1-3.7 wt%), CaO (0.1-1.6 wt%) and TiO<sub>2</sub> contents (0.07-0.57 wt%; Fig. 4). These  
368 lavas are peraluminous with A/CNK ratios in the range 1.03–2.47, and show dominantly alkali-calcic and  
369 magnesian to ferroan affinities. The K<sub>2</sub>O/Na<sub>2</sub>O ratios are higher than 1 (Fig. 7).

370 Rhyolitic lavas display REE patterns with fractionated LREE (2.5<[La/Sm]<sub>n</sub><5.2), with a high variability  
371 of LREE concentrations (38<La<sub>n</sub><730), a lack of HREE fractionation and moderate to pronounced  
372 negative Eu anomaly (0.2<Eu/Eu\*<0.9; Fig. 5B). [Gd/Yb]<sub>n</sub> ratios are generally lower than 1.6, except for  
373 one sample (AWTB34-1; Fig. 5B). The high variability in LREE contents has not been observed in high  
374 field strength elements, then negative Ta- and Nb-anomalies are less important than for intermediate  
375 lavas. But negative Ti-anomaly is systematic and high (Fig. 6B).

376

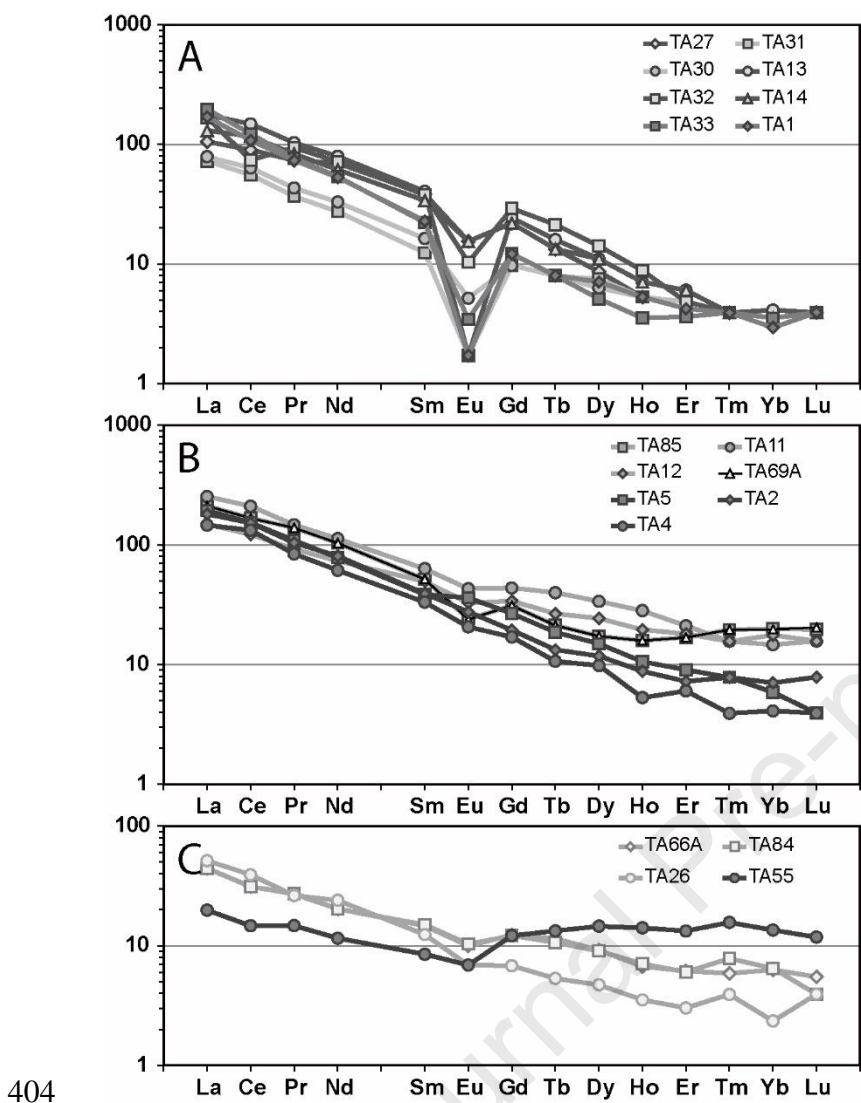
377 **4.2. Tagragra-n-Daouizid area**

378 Rhyolites display major element compositions typical of potassic to high-potassic rhyolites with  $\text{SiO}_2$   
 379 contents ranging between 69.7 and 79.7 wt%,. The high alkali concentrations (> 4 wt%) are essentially  
 380 controlled by  $\text{K}_2\text{O}$  contents (2.2-12.2 wt%; Fig. 4).  $\text{Na}_2\text{O}$  concentrations are always lower than 1 wt%.  
 381 These potassic to highly potassic rhyolites are characterized by negative correlations between  $\text{SiO}_2$  and  
 382  $\text{K}_2\text{O}$ , and with  $\text{Al}_2\text{O}_3$ . The negative correlation between  $\text{SiO}_2$  and  $\text{K}_2\text{O}$  may be related to the presence of  
 383 Si poor and K rich minerals in the source such as ferriferous biotite and/or potassic and ferriferous  
 384 amphibole.

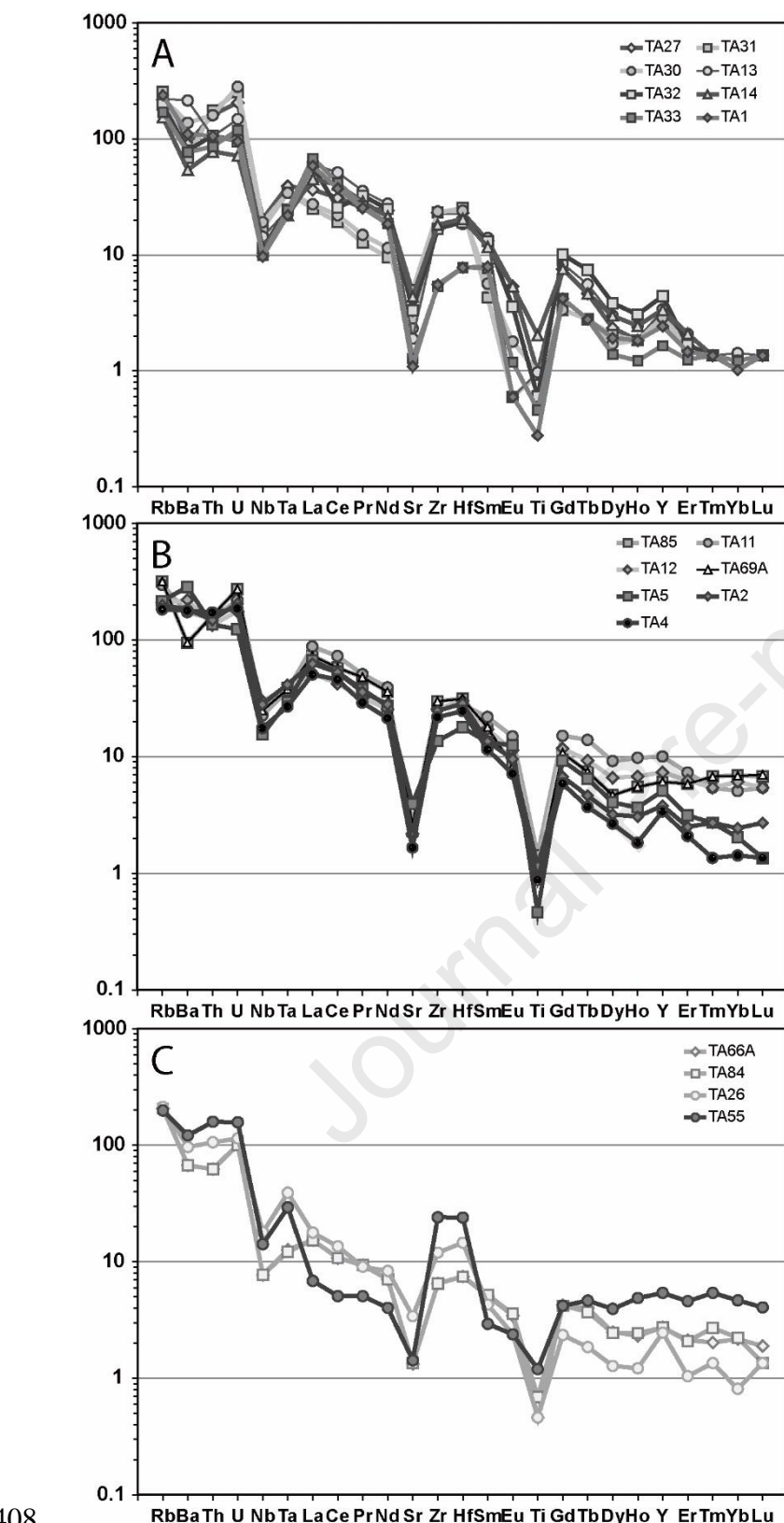
385 Rhyolites display fractionated REE patterns, however four groups may be differentiated (Table 1). In the  
 386 first group,  $[\text{La}/\text{Yb}]_n$  ratios are higher than 20, with fractionated LREE ( $2.7 < [\text{La}/\text{Sm}]_n < 8.9$ ) and HREE  
 387 ( $2.8 < [\text{Gd}/\text{Yb}]_n < 8.3$ ; Fig. 8A), and negative Eu anomalies. HREE contents are lower than 10 times  
 388 chondrites. In the second group (TA5, TA2 and TA4),  $[\text{La}/\text{Yb}]_n$  ratios are higher than 25, with fractionated  
 389 LREE ( $4.4 < [\text{La}/\text{Sm}]_n < 5.0$ ; Fig. 8B) and fractionated HREE ( $2.8 < [\text{Gd}/\text{Yb}]_n < 4.5$ ), without negative Eu-  
 390 anomalies. HREE contents are lower than 10 times chondrites (Fig. 8B). In the third group (TA85, TA11,  
 391 TA12 and TA69A),  $[\text{La}/\text{Yb}]_n$  ratios are lower than 18, with fractionated LREE ( $3.0 < [\text{La}/\text{Sm}]_n < 4.1$ ) and  
 392 slightly fractionated HREE ( $1.6 < [\text{Gd}/\text{Yb}]_n < 3.0$ ), with light negative Eu anomalies. HREE contents are  
 393 higher than 10 times chondrites (Fig. 8B). Finally in the fourth group,  $[\text{La}/\text{Yb}]_n$  ratios are lower than 22,  
 394 with fractionated LREE ( $2.3 < [\text{La}/\text{Sm}]_n < 4.1$ ; Fig. 8C) and flat to slightly fractionated HREE  
 395 ( $0.9 < [\text{Gd}/\text{Yb}]_n < 2.9$ ). These samples are characterized by low REE contents ( $\sum \text{REE} < 60 \text{ ppm}$ ).

396 In sample TA69A, the  $[\text{La}/\text{Yb}]_n$  ratio is lower than 11, with fractionated LREE ( $\text{La}/\text{Sm}]_n=4.1$ ) and slightly  
 397 fractionated HREE ( $[\text{Gd}/\text{Yb}]_n=1.6$ ), with slight negative Eu anomalies. This pattern is similar to sample  
 398 TA85, suggesting that these two rhyolitic ignimbrites represent the same pyroclastic flow. In sample  
 399 TA66A, the  $[\text{La}/\text{Yb}]_n$  ratio is lower than 11, with fractionated LREE ( $\text{La}/\text{Sm}]_n=3.0$ ) and slightly fractionated  
 400 HREE ( $[\text{Gd}/\text{Yb}]_n=2.0$ ), with light negative Eu anomalies. This pattern is similar to sample TA84,  
 401 suggesting that these two rhyolitic ignimbrites represent the same pyroclastic flow.

402 In the Primitive Mantle normalizing diagram (Fig. 9), patterns display systematic negative anomalies in  
 403 Ti and Sr, and sometimes in Nb and Ta.



404  
**Figure 8:** Chondrite normalized rare earth element diagram of volcanic rocks from the Tagragra-n-  
405 Daouizid area. **A.** Group 1 rhyolites; **B.** Groups 2 and 3 rhyolites; **C.** Group 4 rhyolites. Normalization  
406 according to Sun and McDonough, 1989.  
407



408  
409 **Figure 9:** Primitive Mantle normalized multi-element diagram of volcanic rocks from the Tagragra-n-  
410 Daouizid area. **A.** Group 1 rhyolites; **B.** Groups 2 and 3 rhyolites; **C.** Group 4 rhyolites. Normalization  
411 according to Sun and McDonough, 1989.

412 **4.3. Tagragra Ouhallal area**

413 LOI of basaltic trachy-andesites and trachy-andesites are high, however we did not observe significative  
 414 correlation between LOI and an excess or a loss in alkali elements. The compositions are representative  
 415 of the original magma. Major elements variations are illustrated in Figure 4 using silica variations  
 416 diagrams. These lavas have intermediate compositions ( $\text{SiO}_2=52.7\text{-}59.1 \text{ wt\%}$ ), with high  $\text{Al}_2\text{O}_3$  (16-  
 417 21 wt%), intermediate to high  $\text{Fe}_2\text{O}_3$  (6.2-8.6 wt%) and  $\text{K}_2\text{O}$  contents (2.7-5.3 wt%), low to intermediate  
 418  $\text{MgO}$  (1.7-5.6 wt%), and  $\text{Na}_2\text{O}$  (1.8-5.7 wt%), and low  $\text{CaO}$  contents (0.9-3.5 wt%). These rocks are  
 419 alkaline and Ti-rich (0.75-1.47 wt%), with magnesian affinities (Fig. 7).

420 Basaltic trachyandesites and trachyandesites display REE patterns characterized by fractionated LREE  
 421 ( $1.4 < [\text{La}/\text{Sm}]_n < 7.6$ ) and highly fractionated HREE ( $5.0 < [\text{Gd}/\text{Yb}]_n < 11.0$ ) without negative Eu anomalies.  
 422 HREE are lower than ten times chondrites ( $[\text{Yb}]_n = 1.8\text{-}4.7$ ; Fig. 5C). In the Primitive Mantle normalizing  
 423 diagram (Fig. 6C), patterns do not display systematic negative anomalies in Ta and Nb.  
 424 Rhyolites display major element compositions typical of potassic to high-potassic rhyolites with  $\text{SiO}_2$   
 425 contents ranging between 71.8 to 85.3 wt%, and alkali concentrations control essentially by  $\text{K}_2\text{O}$   
 426 contents (2.6-4.7 wt%; Fig. 4).

427 **5. Discussion**428 **5.1. Summary of the depositional environment**

429 In the Tafeltast area, the Ouarzazate Group is essentially composed of terrigenous sediments with few  
 430 volcano-sedimentary rocks and pyroclastic deposits. These sedimentary deposits are located in narrow  
 431 grabens controlled by syn-sedimentary normal faults, and were formed in fluvial-lacustrine system. This  
 432 lacustrine sedimentation is characterized by a maximum flooding outlined by the development of a  
 433 carbonate key bed, the Agoujgal carbonates.

434 In the Tagragra-n-Daouizid area, the Ouarzazate Group represents the surficial emission of a rhyolitic  
 435 magma in pyroclastic flows. Effusive flows or domes are missing. This pyroclastic eruptive activity,  
 436 probably very brief in time, was closely associated with continental sedimentary deposits, mostly coarse  
 437 brecciated or conglomeratic.

438 In the Tagragra Ouahallal area, the massive ash layers at the base of the sequence, the intrusive pillow  
 439 lavas in waterlogged deposits, the stacking of lava flows, the geographical distribution of the flows on

440 one side and of the pillow lavas on the other side, the frequent alternation of emerged and submerged  
 441 periods under shallow water, are quite comparable to that described in subglacial mafic volcanoes  
 442 (Smellie and Skilling, 1994; Skilling, 1994); However, such a depositional environment is not observed  
 443 in the other areas where the depositional system is almost systematically fluvial-lacustrine.

444 In the neighboring Kerdous inlier, Upper Ediacaran rocks are essentially volcaniclastic rocks and rhyolitic  
 445 lavas and domes (O'Connor, 2010). Upper Ediacaran sedimentary, volcaniclastic and volcanic rocks  
 446 have been divided in three main groups: i) Oufoud; ii) Tanalt; and iii) Fiyzirt (O'Connor, 2010). On the  
 447 southern border of the Kerdous inlier, the Oufoud Group, characterized by a dominantly conglomeratic  
 448 sequence with rhyodacitic lava and ignimbrite. In the centre of the Kerdous inlier, the Tanalt Group  
 449 comprises a succession of matrix-supported conglomerate, coarse-grained to well-bedded fine  
 450 sandstone and siltstone, with locally interbedded rhyolitic welded pyroclastic tuff. On the eastern border  
 451 of the Kerdous inlier, the Fiyzirt Group comprises conglomerate, sandstone, basaltic lava and shallow  
 452 level intrusion. Lavas and tuffs were emplaced throughout the sedimentary rocks which were deposited  
 453 in a subaerial environment, probably on alluvial fan and flood plains with local shallow lakes (O'Connor,  
 454 2010). Geochemically, volcanic rocks have high-K calc-alkaline to alkaline affinities, characteristics of  
 455 both subduction and within-plate tectonic settings (O'Connor, 2010).

456 In the Bas Draâ inlier, the volcanic activity evolved in a continental extensional setting (Karaoui et al.,  
 457 2014). The Ouarzazate Group is characterized by four distinct units (Karaoui et al., 2014): i) rhyolitic  
 458 ignimbrite; ii) rhyolitic lava-dome and basaltic andesite scoria cone, with rare ignimbrite; iii) basaltic to  
 459 basaltic andesite lavas with minor pyroclastic deposits; and iv) rhyolitic lava-dome. Sedimentary  
 460 processes are characteristics of fluvial systems, and the lack of volcanosedimentary mass flow deposits  
 461 indicates a low relief environment (Karaoui et al., 2014). Geochemically, volcanic rocks have high-K  
 462 calc-alkaline, alkali-calcic and alkaline affinities, characteristics of both subduction and within-plate  
 463 tectonic settings (Karaoui et al., 2014).

## 464 **5.2. Tectonic discrimination diagrams**

465 Geochemical data of the mafic to intermediate lavas from the Kerdous inlier and the Tagragra Ouhallal  
 466 area provide important informations regarding their tectonic setting. On the Y/15–La/10–Nb/8 diagram  
 467 (Fig. 10), mafic lavas from the Kerdous inlier and the Tagragra Ouhallal area fall in the calc-alkaline  
 468 basalt and continental tholeiite fields. Like these lavas, basalts from the Bas Draâ (Karaoui et al., 2014)

469 and Agadir-Melloul (Blein et al., 2014b) inliers fall in the fields of calc-alkaline basalts and continental  
 470 tholeiites. Basalts from the southwestern or northeastern flank of the Kerdous inlier (Soulaimani et al.,  
 471 2004) fall on the boundary between the fields of the continental tholeiites and back-arc basalts. These  
 472 Upper Ediacaran basalts are distinguished from the Cambrian basalts of the jbel Boho (Bou Azer inlier;  
 473 Benouada et al., 2017) which have an affinity of alkaline basalts to continental tholeiites. The Upper  
 474 Ediacaran mafic rocks show a clear south-north evolution from continental tholeiites to back-arc basalts,  
 475 characterized by a relative enrichment in Y compared to La and Nb. This volcanic activity occurred  
 476 during an extensional episode, certainly more important in the north than in the south because the  
 477 mantle source has a more asthenospheric signature in the north than in the south.

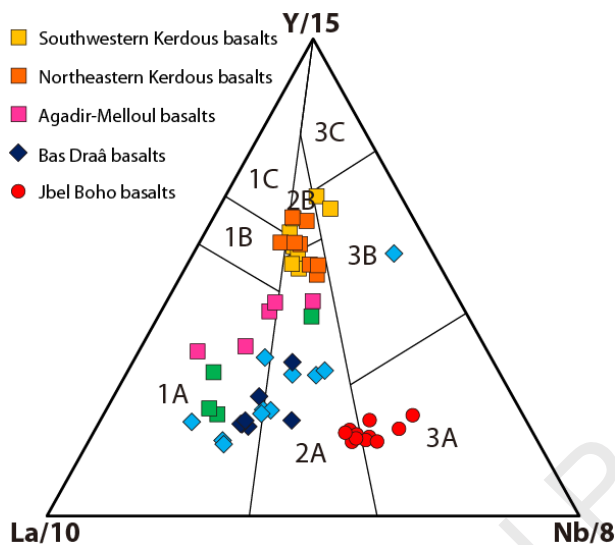
478 As shown in Figure 11 ( $\text{FeO}^t+\text{MgO}$  versus  $\text{Nb}+\text{Zr}+\text{Y}$ ,  $\text{La}_n$  and  $\text{Sr}+\text{Ba}$ ), intermediate to felsic rocks can  
 479 be classified into two main groups: i) low  $\text{FeO}^t+\text{MgO}$  (<7 wt.%) metaluminous to peraluminous rocks,  
 480 with moderate incompatible element contents, generated mainly by partial melting of crustal lithologies;  
 481 and ii) high  $\text{FeO}^t+\text{MgO}$  (>7 wt.%) metaluminous intermediate to felsic rocks with moderate incompatible  
 482 element contents, generated by an enriched mantle source with variable involvement of crustal  
 483 component.

484 Whalen and Hildebrand (2019) developed new diagrams to discriminate between arc, slab-failure and  
 485 A-type granitoids. These diagrams are valid for non peraluminous samples ( $\text{ASI} < 1.1$ ), with  $\text{SiO}_2$   
 486 concentrations ranging between 55 and 70 wt%. Samples from the Ouarzazate Group that meet these  
 487 criteria have been plotted in such diagrams (Fig. 12A-B).

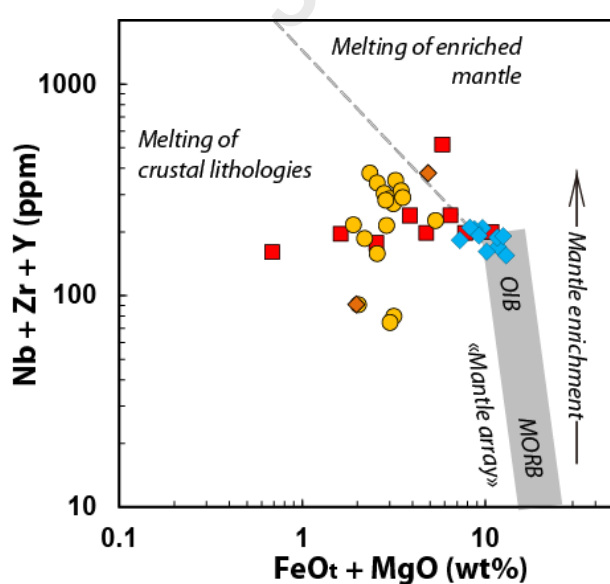
488 With high  $\text{Nb}/\text{Y}$ ,  $\text{Gd}/\text{Yb}$ , and  $\text{La}/\text{Yb}$  ratios, samples from Tagragra Ouhallal plot in the slab-failure field,  
 489 while samples from the Kerdous and Agadir-Melloul inliers, with lower  $\text{Nb}/\text{Y}$ ,  $\text{La}/\text{Yb}$  and  $\text{Gd}/\text{Yb}$  ratios  
 490 and plot at the limit between arc and slab-failure fields (Fig. 12A-B). As typical characteristic of magmas  
 491 generated by slab-failure, samples from Tagragra Ouhallal have low  $\text{Ta}+\text{Yb}$  values (Fig. 12B). All  
 492 samples have  $\text{Ta}/\text{Yb}$  ratios higher than 0.3., and plot in the field of slab-failure magmas (Fig. 12B). Their  
 493 high  $\text{La}/\text{Yb}$  (>10), and  $\text{Nb}/\text{Y}$  (>0.4) ratios are typical of slab-failure rocks (Fig. 12A-B). Samples from the  
 494 Kerdous and Agadir-Melloul inliers, and the Tagragra-n-Daouizid area, with higher  $\text{Ta}+\text{Yb}$  values, and  
 495 lower  $\text{La}/\text{Yb}$ , and  $\text{Nb}/\text{Y}$  ratios than samples from the Tagragra Ouhallal area. In Figure 12A-B, they plot  
 496 at the limit between arc and slab-failure fields.

497 On  $\text{Y}$  vs.  $\text{Nb}$  and  $\text{Yb}$  vs.  $\text{Ta}$  diagrams (Fig. 12C-D), the samples from the Tagragra Ouhallal and  
 498 Tagragra-n-Daouizid areas also plot in the slab-failure field, while samples from the Kerdous inlier plot

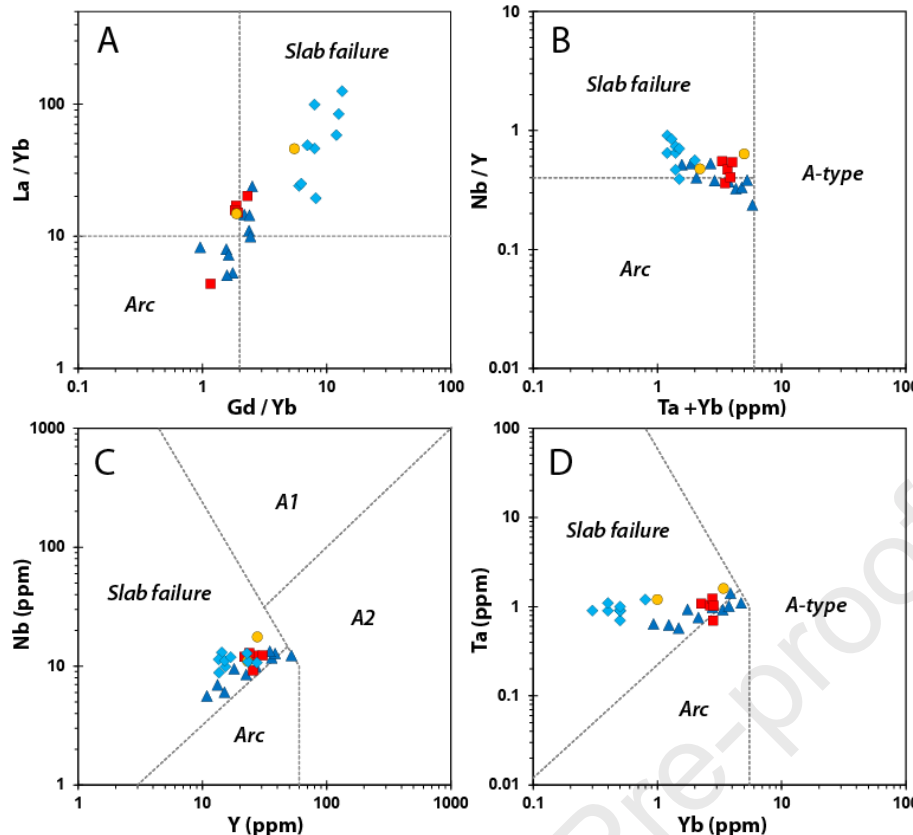
499 close to the triple point between arc, slab-failure and A-type fields, which is characteristic of granites  
 500 formed in post-collisional extensional settings (Förster et al., 1997).  
 501 Geochemical data indicate that: (i) mafic rocks are essentially continental flood basalt; (ii) felsic rocks  
 502 are high-K calc-alkaline rocks, generated by partial melting of an enriched mantle source with  
 503 involvement of crustal component; and (iii) few intermediate and felsic rocks sharing characteristics with  
 504 slab failure magma (Hildebrand and Whalen, 2017).



505  
 506 **Figure 10:** Y/15–La/10–Nb/8 diagram (Cabanis and Lecolle, 1989) for mafic rocks ( $\text{SiO}_2 < 55 \text{ wt\%}$ ) of  
 507 the Ouarzazate Group (1A: Calc-alkaline basalts; 1B: Calc-alkaline basalts and arc tholeiites; 1C:  
 508 Volcanic arc tholeiites; 2A: Continental tholeiites; 2B: Back-arc basalts; 3A: Alkaline basalts; 3B: E-type  
 509 MORB; 3C: N-type MORB; Symbols as in Fig. 3).



510  
 511 **Figure 11:**  $(\text{FeO}^t + \text{MgO})$  vs.  $(\text{Nb} = \text{Zr} + \text{Y})$  diagram (Symbols as in Fig. 3).



512

513 **Figure 12:** Discrimination diagrams showing slab failure, A-type and arc fields (Hildebrand and Whalen,  
 514 2014; Hildebrand et al., 2018; Whalen and Hildebrand, 2019). Samples, plotted on diagrams, have  $\text{SiO}_2$   
 515 contents between 55 and 70 wt%, and alumina saturation index (ASI) value lower than 1.1: **A.**  $\text{Gd}/\text{Yb}$  vs  
 516  $\text{La}/\text{Yb}$ ; **B.**  $\text{Ta}+\text{Yb}$  vs.  $\text{Nb}/\text{Y}$ ; **C.**  $\text{Y}$  vs.  $\text{Nb}$ ; and **D.**  $\text{Yb}$  vs.  $\text{Ta}$ . Symbols as in Fig. 3. Light blue triangle:  
 517 Ouarzazate Group from the Agadir Melloul inlier (Blein et al., 2014b).

### 518 5.3. Geodynamic setting

519 Thomas et al. (2004) divided the Neoproterozoic igneous rocks of the Anti-Atlas belt in two main  
 520 supergroups: Anti-Atlas and Ouarzazate supergroups. The lithostratigraphic units of the Anti-Atlas  
 521 Supergroup are related to passive margin, oceanic and island-arc development phases of the Pan  
 522 African orogen before ca. 650 Ma. All the younger plutonic, volcanic and sedimentary rocks have been  
 523 grouped into the Ouarzazate Supergroup. The pre 580 Ma volcano-sedimentary rocks of the Ouarzazate  
 524 Supergroup were deposited in narrow strike-slip pull-apart basins (Saghro, Bou Salda, Mgouna, Tafrawt  
 525 and Anzi groups) contemporaneously with high-K calc-alkaline plutons (e.g., Assarag, Bardouz Suites).  
 526 These rocks were followed by the unconformable continental deposition of voluminous pyroclastic  
 527 deposits and volcano-sedimentary rocks (the Ouarzazate Group); the volcanic rocks were erupted from  
 528 several volcanic centers and caldera complexes, and are younger than 580 Ma (Thomas et al., 2002;

529 El Baghdadi et al., 2003; Gasquet et al., 2005, 2008; Errami et al., 2009; Toummite et al., 2012; Walsh  
 530 et al., 2012; Blein et al., 2014b; Baidada et al., 2017; Belkacim et al., 2017).

531 Set up between ca. 575 and ca. 545 Ma, the Ouarzazate Group can be subdivided into three major  
 532 magmatic pulses dated between: (i) 575 and 570 Ma, (ii) 568 and 563 Ma, (iii) and 555 and 545 Ma. In  
 533 the Agadir-Melloul inlier, Blein et al. (2014b) highlighted angular unconformities between each volcanic  
 534 pulses. The first unconformity is placed around ca. 568 Ma and the younger at ca. 560 Ma. The latter  
 535 angular unconformity has been described in the Saghro massif (Walsh et al., 2012), and in the western  
 536 Anti-Atlas (Blein et al., 2014b). Finally, the last one is in continuity with the sedimentary rocks of the  
 537 Adoudou Formation. A complete stratigraphy of these three pulses has been observed in the Agadir-  
 538 Melloul inlier (Blein et al., 2014b) and in the Saghro massif (Errami et al., 2020; Yajoui et al., 2020).

539 In the Saghro massif, before the deposition of the Ouarzazate Group, Imiter and Iknoun granodiorites  
 540 (600–603 Ma) were uplifted and exhumed. The Oussilkane charnockite, dated at  $580 \pm 19$  Ma (Errami et  
 541 al., 2020), is contemporaneous with this phase of uplift. In the Bou Azer inlier, the ignimbrites of the  
 542 Ouarzazate Group were deposited unconformably on the volcano-sedimentary sequence of the Tiddilene  
 543 Group (602–606 Ma), and on the uplifted and exhumed Bleïda granodiorite ( $579 \pm 2$  Ma; Inglis et al.,  
 544 2004). These observations suggest the occurrence of an uplift between ca. 580 and ca. 575 Ma.

545 Late Ediacaran geodynamic models are the subject of much debate. A scenario suggest the occurrence  
 546 of a subduction ca. 625–560 Ma to explain the Ouarzazate high-K calc-alkaline magmatism (El Baghdadi  
 547 et al., 2003; Benziane, 2007; Walsh et al., 2012; Hefferan et al., 2014). Another scenario suggest a post-  
 548 collisional transtensional setting, without subduction, for the late Ediacaran Pan-African orogeny (Doblas  
 549 et al., 2002; Thomas et al., 2002; Gasquet et al., 2005; Karaoui et al., 2015). Blein et al. (2014b) propose  
 550 a subduction beneath the WAC ca. 625–580 Ma, followed by the arrival of a spreading ridge at the  
 551 subduction zone at ca. 580–575 Ma, and post ca. 575 Ma by the pyroclastic magmatism in a  
 552 transtensive setting (Ouarzazate Group).

553 Tuduri et al. (2018) put forward a closer model with the development of a subduction between 610 and  
 554 575 Ma, followed by the initiation of a slab roll-back around ca. 575 Ma. This slab roll-back results in  
 555 large volume of magma, leading to the pyroclastic flows of the Ouarzazate Group. And ongoing slab  
 556 roll-back along with more extensional tectonic setting initiate the second, and then the third ignimbritic  
 557 pulses (Tuduri et al., 2018).

558 Dominated by the eruptions of thousands of cubic kilometers of pyroclastic flows, volcanic activity of the  
 559 Ouarzazate Group is typical of ignimbrite flare-ups. Originally, flare-ups are short-lived large volumes of  
 560 silicic ignimbrites in orogenic setting, inland from the plate margin (Lipman et al., 1971; Noble, 1972).  
 561 These flare-ups are intercalated in the stable magmatism of an active margin, characterized by andesitic  
 562 volcanic and intrusive rocks. This stable active margin magmatism is characterized by low magmatic  
 563 addition rates (MAR). Flare-ups are typically short-time high-MAR episodes, alternating with longest  
 564 low-MAR episodes.

565 High-resolution zircon geochronological ages reveal multiple events and the intermittent nature of flare-  
 566 ups at various scales of space, time, and volumes (Folkes et al. 2011; Lima et al. 2012; Silva et al.,  
 567 2015). Considered as a primary pulse, the flare-up or high-volume event is a 40-50 my mantle activity  
 568 induced by: (i) post-collisional mantle delamination (Ducea, 2001), (ii) a regional transition from low-  
 569 angle to high-angle plate convergence in relation to slab roll-back (Lipman et al., 1972; Best et al., 2013),  
 570 or (iii) slab breakoff (Ferrari et al., 2002). This primary pulse can be broken down in secondary pulses.  
 571 These shorter secondary pulses (~10–20 my) must reflect the timescale of melt production and delivery  
 572 from the melting and assimilation zone, and its interaction with the upper crust (de Silva et al., 2015).  
 573 Typically observed in Andean volcano-plutonic systems, such 10 my secondary pulses are an essential  
 574 signal in orogenic magmatic activity (Coleman et al., 2004; Grunder et al., 2008). Due to its duration  
 575 (~30–35 my), the pyroclastic volcanism of the Ouarzazate Group is a typical primary pulse, the three  
 576 ignimbritic pulses observed in Agadir Melloul (Adrar-n-Takoucht, Tadoughast and Fajjoud formations)  
 577 and Imiter (~10 my in duration) are typically secondary pulses.

578 According to DeCelles et al. (2009), flare-ups are periods of high rates of magma production, relative to  
 579 the normal state rates of arc-magma production. A transition from low-angle to high-angle plate  
 580 convergence in relation to slab roll-back may explain such higher magmatic fluxes, and episodic  
 581 alternations between magmatic lulls and flare ups (Ferrari et al., 2007). In the Anti-Atlas, the late  
 582 Ediacaran magmatic activity is not characterized by episodic alternations between normal arc-magma  
 583 production and flare up activity, but by an individual flare up event predating the development of a  
 584 Cambrian marine carbonate platform (Alvaro et al., 2014). There are many mechanisms to explain such  
 585 individual flare up events such as: (i) slab break-off (e.g., Schwartz et al., 2017), (ii) subduction of  
 586 fracture zones (e.g., Manea et al., 2014), or (iii) subduction of continental lithospheric mantle before a  
 587 collision (e.g., Ganade et al., 2021). In our case, the late Ediacaran flare up event is related to a slab

588 break-off event. As the late Ediacaran Ouarzazate magmatism is not followed by a continental collision  
 589 event, it cannot be related to the subduction of continental lithospheric mantle, and the late Ediacaran  
 590 flare up event is widespread, and not geographically restricted like in subduction of fracture zones.  
 591 Moreover, volcanic rocks of the Ouarzazate Group fall in the field of slab-failure rocks (Fig. 11).

592 **6. Conclusions**

593 New constraints on the late Ediacaran evolution of the western Anti-Atlas New have been provided from  
 594 geological mapping, petrography and geochemistry of volcano-sedimentary rocks of the southern  
 595 Kerdous and Tagragra d'Akka inliers.

596 In the Kerdous and Tagragra d'Akka inliers, the Ouarzazate Group consists of terrigenous sediments,  
 597 volcano-sedimentary rocks, basaltic flows and dacitic to rhyolitic, welded or unwelded, pyroclastic tuffs.  
 598 These deposits are located in grabens controlled by syn-sedimentary normal faults. The sedimentation  
 599 is characterized by a maximum flooding outlined by the Agoujgal carbonates. Dacitic to rhyolitic  
 600 pyroclastic tuffs of the Ouarzazate Group have a high-potassic calc-alkaline affinity. Basalts observed  
 601 in the Kerdous inlier and the Tagragra Ouahallal area have transitional affinity between continental  
 602 tholeiites and calc-alkaline basalts. Few intermediate and felsic volcanic rocks are characteristics of slab  
 603 failure rocks derived from melting of mafic upper portion of the subducted slab (Hildebrand and Whalen,  
 604 2017).

605 The Ouarzazate flare up event is related to the cessation of a subduction, which induced a slab break-  
 606 off. The late Ediacaran Ouarzazate magmatism in not followed by a continental collision event, and  
 607 cannot be related to the subduction of continental mantle lithosphere; the late Ediacaran flare up event  
 608 is widespread, and not geographically restricted like in subduction of fracture zones.

609

610 **Credit authorship contribution statement**

611 Olivier Blein: Interpretation of chemical data and wrote the manuscript. Thierry Baudin, Philippe  
 612 Chèvremont, and Dominique Gasquet: Contributed in the field work, sampling, and to the writing of the  
 613 manuscript.

614 **Declaration of competing interest**

615 The authors declare that they have no known competing financial interests or personal relationships that  
 616 could have appeared to influence the work reported in this paper.

617 **Acknowledgements**

618 Funding was provided by the Moroccan Ministry of Energy, Mines, Water and Environment (contracts  
 619 19-2008/DG) with the production of geological four mapsheets and explanatory notes (Sidi Bou'Addi,  
 620 Awkarda, Tamazrar, Tlatat Ida Gougmar).

621 **References**

- 622 Abati, J., Aghzer, A.M., Gerdes, A., Ennih, N., 2010. Detrital zircon ages of Neoproterozoic sequences  
 623 of the Moroccan Anti-Atlas belt. *Precambrian Research* 181, 115–128.  
 624 <https://doi:10.1016/j.precamres.2010.05.018>.
- 625 Aït Lahna, A., Youbi, N., Tassinari, C.C.G., Basei, M.A.S., Ernst, R.E., Chaib, L., Barzouk, A., Mata, J.,  
 626 Gärtner, A., Admou, H., Boumehdi, M.A., Söderlund, U., Bensalah, M.K., Bodinier, J.L., Maacha,  
 627 L., Bekker, A., 2020. Revised stratigraphic framework for the lower Anti-Atlas supergroup based on  
 628 U-Pb geochronology of magmatic and detrital zircons (Zenaga and Bou Azzer-El Graara inliers,  
 629 Anti-Atlas Belt, Morocco), *J. Afr. Earth Sci.* 171, 103946.  
 630 <https://doi:10.1016/j.jafrearsci.2020.103946>.
- 631 Aït Malek, H., Gasquet, D., Bertrand, J. M., Leterrier J., 1998. Géochronologie U-Pb sur les  
 632 granitoïdes éburnéens et panafricains dans les boutonnières protérozoïques d'Igherm, du Kerdous  
 633 et du Bas Drâa (Anti-Atlas occidental, Maroc). *Comptes Rendus de l'Académie des Sciences* 327,  
 634 819–826. [https://doi:10.1016/S1251-8050\(99\)80056-1](https://doi:10.1016/S1251-8050(99)80056-1).

- 635 Alvaro, J.J., Clausen, S., El Albani, A., Chellai, E.H., 2005. Facies distribution of Lower Cambrian  
 636 cryptic microbial and epibenthic archaeocyathan–microbial communities in the western Anti-Atlas,  
 637 Morocco. *Sedimentology*, 53, 35–53. <https://doi:10.1111/j.1365-3091.2005.00752.x>.
- 638 Álvaro, J.J., Bellido, F., Gasquet, D., Francisco Pereira, M., Quesada, C., Sánchez-García, T., 2014.  
 639 Diachronism in the late Neoproterozoic–Cambrian arc-rift transition of North Gondwana: A  
 640 comparison of Morocco and the Iberian Ossa-Morena Zone. *Journal of African Earth Sciences* 98:  
 641 113–132.
- 642 Baidada, B., Cousens, B., Alansari, A., Soulaimani, A., Barbey, P., Ilmen, S., Ikenne, M., 2017.  
 643 Geochemistry and Sm-Nd isotopic composition of the Imiter Pan-African granitoids (Saghro massif,  
 644 eastern Anti-Atlas, Morocco): Geotectonic implications. *J. Afr. Earth Sci.* 127, 99–112.  
 645 <https://doi:10.1016/j.jafrearsci.2016.08.016>.
- 646 Bajja, A., 1998. Volcanisme syn à post-orogénique du Néoprotérozoïque de l'Anti-Atlas: implications  
 647 pétrographiques et géodynamiques (Thèse de doctorat d'Etat). Université Chouaib Doukkali, El  
 648 Jadida, Maroc (215 p.).
- 649 Bajja, A., 2001. Volcanisme syn a post orogénique du Néoprotérozoïque de l'Anti-Atlas: implications  
 650 pétrogénétiques et géodynamiques. In: De Wall, H., Greiling, R.P. (Eds.), *Magmatic Evolution of a*  
 651 *Neoproterozoic island-Arc syn-to Post-orogenic Igneous Activity in the Anti-Atlas (Morocco)*,  
 652 Forschungszentrum Jülich GmbH, vol. 45, pp. 9–228.
- 653 Baudin, T., Razin, P., Chèvremont, P., Calvès, G., Gabudianu, D., Roger, J., 2005. Carte géol. Maroc  
 654 (1/50 000), feuille Awkarda. Notes et Mémoires Serv. Géol., Maroc, n°497.
- 655 Belkacim, S., Gasquet, D., Liégeois, J.P., Arai, S., Ghalan, H., Ahmed, H.A., Ishida, Y., Ikenne, M.,  
 656 2017. The Ediacaran volcanic rocks and associated mafic dykes of the Ouarzazate Group (Anti-  
 657 Atlas, Morocco): Clinopyroxene composition, whole-rock geochemistry and Sr-Nd isotopes  
 658 constraints from the Ouzellarh-Sirwa salient (Tifnoute valley). *J. Afr. Earth Sci.* 127, 113–135.  
 659 <https://doi:10.1016/j.jafrearsci.2016.08.002>
- 660 Benaouda, R., Holzheid, A., Schenk, V., Badra, L., Ennaciri, A., 2017. Magmatic evolution of the Jbel  
 661 Boho alkaine complex in the Bou Azzer inlier (Anti-Atlas, Morocco) and its relation to REE  
 662 mineralization. *J. Afr. Earth Sci.* 129; 202–223. <https://doi:10.1016/j.jafrearsci.2017.01.003>.

- 663 Bensaou, M., Hamoumi, N. 2001. L'Anti-Atlas occidental du Maroc: étude sédimentologique et  
 664 reconstitutions paléogéographiques au Cambrien inférieur. *J. Afr. Earth Sci.* 32, 351–372.  
 665 [https://doi:10.1016/S0899-5362\(01\)90102-2](https://doi:10.1016/S0899-5362(01)90102-2)
- 666 Bensaou, M., Hamoumi, N. 2003. Le graben de l'Anti-Atlas occidental (Maroc) : contrôle tectonique  
 667 de la paléogéographie et des séquences du Cambrien inférieur. *C.R. Géoscience* 335, 297–305.  
 668 [https://doi:10.1016/S1631-0713\(03\)00033-6](https://doi:10.1016/S1631-0713(03)00033-6)
- 669 Benziane, F., 2007. Lithostratigraphie et évolution géodynamique de l'Anti-Atlas (Maroc) du  
 670 Paléoprotérozoïque au Néoprotérozoïque: exemples de la boutonnière de Tagagra de Tata et du  
 671 Jbel Saghro. PhD thesis. Université de Savoie CISM, Chambéry, France, 320 pp.
- 672 Best, M.G., Christiansen, E.H., Gromme, S., 2013. Introduction: the 36–18 Ma southern Great Basin,  
 673 USA, ignimbrite province and flare up: swarms of subduction-related supervolcanoes. *Geosphere*  
 674 9: 260–274.
- 675 BGS, 2001a. Carte géologique du Had-n-Tahala au 1/50 000. Notes et Mémoires, 403, Editions du  
 676 Service Géologique du Maroc, Rabat.
- 677 BGS, 2001b. Carte géologique d'Anzi au 1/50 000. Notes et Mémoires, 402, Editions du Service  
 678 Géologiques du Maroc, Rabat.
- 679 Blein, O., Chèvremont, Ph., Baudin, T., Ouanaimi, H., Razin, Ph., Hafid, A., Admou, H., Soulaimani,  
 680 A., Bouabdelli, M, Abia, E.H., Beni Akhy, R., 2013. Notice explicative carte géol. Maroc (1/50 000),  
 681 feuille Tabadrist, Notes et Mémoires Serv. Géol. Maroc, n°547, MEM/BRGM. Carte géologique par  
 682 Baudin, T., Blein, O., Chèvremont, Ph., Soulaimani, A., Ouanaimi, H., Roger, J., Admou, H., Hafid,  
 683 A., Bouabdelli, M., Abia, E.H., 2013.
- 684 Blein, O., Baudin, T., Chèvremont, P., Soulaimani, A., Admou, H., Gasquet, D., Cocherie, A., Egal, E.,  
 685 Youbi, N., Razin, P., Bouabdelli, M., Gombert, Ph., 2014a. Geochronological constraints on the  
 686 polycyclic magmatism in the Bou Azzer-El Graara inlier (Central Anti-Atlas Morocco). *J. Afr. Earth  
 687 Sci.* 99, 287–306. <https://doi:10.1016/j.jafrearsci.2014.04.021>.
- 688 Blein, O., Baudin, T., Soulaimani, A., Cocherie, A., Chèvremont, P., Admou, H., Ouanaimi, H., Hafid,  
 689 A., Razin, P., Bouabdelli, M., Roger, J., 2014b. New Geochemical, Geochronological and Structural  
 690 Constraints on the Ediacaran Evolution of the South Sirwa, Agadir Melloul and Iguerda Inliers, Anti-  
 691 Atlas, Morocco. *J. Afr. Earth Sci.* 98, 47–71. <https://doi.org/10.1016/j.jafrearsci.2014.06.019>

- 692 Blein, O., Chèvremont, P., Baudin, T., Hafid, A., Admou, H., Soulaimani, A., Ouainami, H., Bouabdelli,  
 693 M., Gasquet, D., Padel, M., 2022. Contrasting Paleoproterozoic granitoids in the Kerdous,  
 694 Tragragrad'Akka, Agadir-Melloul and Iggerda inliers (western Anti-Atlas, Morocco). *J. Afr. Earth  
 695 Sci.* 189, 104500. <https://doi.org/10.1016/j.jafrearsci.2022.104500>
- 696 Boudda, A., Choubert, G., Faure-Muret, A., 1979. Essai de stratigraphie de la couverture sédimentaire  
 697 de l'Anti-Atlas : Adoudounien-Cambrien inférieur. Notes et Mémoires du Service Géologique du  
 698 Maroc 271, 96 p.
- 699 Bouougri, E.H., Saquaque, A., 2004. Lithostratigraphic framework and correlation of the  
 700 Neoproterozoic northern West African Craton passive margin sequence (Siroua – Zenaga - Bou  
 701 Azzer El Graara inliers, central Anti-Atlas, Morocco): an integrated approach. *J. Afr. Earth Sci.* 99,  
 702 287–306. <https://doi:10.1016/j.jafrearsci.2004.07.045>.
- 703 Cabanis, B., Lecolle, M., 1989. Le diagramme La/10-Y/15-Nb/8 : un outil pour la discrimination des  
 704 séries volcaniques et la mise en évidence des processus de mélange et/ou de contamination  
 705 crustale. *C. R. Acad. Sci. Ser. II* 309, 2023–2029.
- 706 Carignan, J., Hild, P., Mévelle, G., Morel, J., Yeghicheyan, D., 2001. Routine analyses of trace  
 707 elements in geological samples using flow injection and low pressure on-line liquid chromatography  
 708 coupled to ICP-MS: a study of reference materials BR, DR-N, UB-N, AN-G and GH. *Geostandards  
 709 Newslett.* 25, 187–198.
- 710 Chalot-Prat, F., Gasquet, D., Roger, J., Hassenforder, B., Chèvremont, P., Baudin, T., Razin, P.,  
 711 Benlakhdim, A., Benssaou, M., Mortaji, A., 2001. Carte géologique du Maroc au 1/50000. Feuille  
 712 de Sidi Bou'Addi avec Mémoire explicatif. Notes et Mémoires du Service Géologique du Maroc 414  
 713 & 414 bis, 84 p.
- 714 Cheilletz, A., Levresse, G., Gasquet, D., Azizi Samir, M.R., Zyadi, R., Archibald, D.A., 2002. The Imitec  
 715 epithermal deposit (Morocco): new petrographic, microtectonic and geochronological data.  
 716 Importance of the Precambrian–Cambrian transition for major precious metals deposits in the Anti-  
 717 Atlas. *Miner. Deposita* 37, 772–781.
- 718 Chèvremont, P., Razin, P., Baudin, T., Gabudianu, D., Roger, J., Thiéblemont, D., Calvès, G., Anzar-  
 719 Conseil, 2005. Notice explicative, carte géol. Maroc (1/50 000), feuille Awkarda, Notes et Mém.  
 720 Serv. Géol. Maroc, n°497bis, MEM/BRGM, 114 p. Carte géol. par Baudin T., Razin P., Chèvremont  
 721 P., Calvès G., Gabudianu D., Roger J. (2005), Notes et Mém. Serv. Géol. Maroc, n°497.

- 722 Chèvremont, P., Blein, O., Razin, P., Simon, B., Baudin, T., Ouanaïmi, H., Soulaimani, A., El Janati,  
 723 M., Bouabdelli, M., Abia, E.H., Admou, H., Hafid, A., Beni Akhy, R., 2013. Notice explicative carte  
 724 géol. Maroc (1/50 000), feuille Ighriy, Notes et Mémoires Serv. Géol. Maroc, n°548, MEM/BRGM.  
 725 Carte géologique par Ouanaïmi, H., Chèvremont, Ph., Blein, O., Simon, B., Baudin, T., Razin, Ph.,  
 726 Smektala, F., Soulaimani, A., El Janati, M., Abia, E.H., Admou, H., Hafid, A., Bouabdelli, M., 2013.  
 727 Choubert, G., 1952. Histoire géologique du domaine de l'Anti-Atlas. In: Géologie du Maroc. Notes et  
 728 Mémoires du Service Géologique du Maroc 100, 75–194.  
 729 Choubert, G., 1953a. Histoire géologique du domaine de l'Anti-Atlas. Notes et Mémoire de Service  
 730 géologique du Maroc 100, 1–77.  
 731 Choubert, G., 1953b. Le Précambrien III et le Géorgien de l'Anti-Atlas. Notes et Mémoire de Service  
 732 géologique du Maroc 103, 7–39.  
 733 Choubert, G., 1963. Histoire géologique du Précambrien de l'Anti-Atlas. Notes et Mémoires du Service  
 734 Géologique du Maroc 162, 443 p.  
 735 Choubert, G., Faure-Muret, A., 1970. Colloque international sur les corrélations du Précambrien,  
 736 Agadir-Rabat, 3–23 mai 1970, et livret-guide de l'excursion: Anti-Atlas occidental et central, Notes  
 737 Mém. Serv. Géol. Maroc 229, 259p.  
 738 Choubert, G., Boudda, A., Faure-Muret, A., 1973. Essai de Chronologie du Précambrien supérieur du  
 739 sud marocain: C. R. Somm. S.G.F, 123–124.  
 740 Clauer, N., 1976. Géochimie isotopique du Strontium des milieux sédimentaires. Application à la  
 741 géochronologie de la couverture du Craton Ouest-Africain. Strasbourg.  
 742 Coleman, D.S., Glazner, A.F., 1997. The Sierra Crest magmatic event: rapid formation of juvenile  
 743 crust during the Late Cretaceous in California. International Geology Review 39: 768–787.  
 744 DeCelles, P.G., Ducea, M.N., Kapp, P., Zandt, G., 2009. Cyclicity in Cordilleran orogenic systems.  
 745 Nature Geoscience 2: 251–257  
 746 De Silva, S.L., Riggs, N.R., Barth, A.P., 2015. Quickening the pulse: Fractal tempos in continental arc  
 747 magmatism. Elements 11, 113–118. <https://doi:10.2113/gselements.11.2.113>.  
 748 D'Lemos, R.S., Inglis, J.D., Samson, S.D., 2006. A newly discovered orogenic event in Morocco:  
 749 Neoproterozoic ages for supposed Eburnean basement of the Bou Azzer inlier, Anti-Atlas  
 750 Mountains. Precambrian Research 147, 65–78.

- 751 Doblas, M., Lopez-Ruiz, J., Cebria, J.M., Youbi, N., Degroote, E., 2002. Mantle insulation beneath the  
 752 west African craton during the Precambrian–Cambrian transition. *Geology* 30, 839–842.
- 753 Ducea, M., 2001. The California arc: thick granitic batholiths, eclogitic residues, lithospheric-scale  
 754 thrusting, and magmatic flare-ups. *GSA Today* 11, 4–10.
- 755 Ducrot, J., Lancelot, J.R., 1977. Problème de la limite Précambrien-Cambrien : étude radio-  
 756 chronologique par la méthode U-Pb sur zircons du volcan du Jbel Boho (Anti-Atlas Marocain).  
 757 *Canadian Journal of Earth Sciences* 14, 2771–2777.
- 758 Eddif, A., Gasquet, D., Hoepffner, C., Levresse, G., 2007. Age of the Wirgane granodiorite intrusions  
 759 (Western High Atlas, Morocco): new U–Pb constraints. *J. Afr. Earth Sci.* 47, 227–231.
- 760 El Baghdadi, M., El Boukhari, A., Jouider, A., Benyoucef, A., Nadem, S., 2003. Calc-alkaline arc I-type  
 761 granitoid associated with S-type granite in the Pan-African belt of eastern Anti-Atlas (Saghro and  
 762 Ougnat, South Morocco). *Gondwana Res.* 6 (4), 557–572. [https://doi:10.1016/S1342-937X\(05\)71007-8](https://doi:10.1016/S1342-937X(05)71007-8).
- 763  
 764 Ennih, N., Liégeois, J.-P., 2008. The boundaries of the West African Craton, with special reference to  
 765 the basement of the Moroccan metacratonic Anti-Atlas belt. Geological Society, London, Special  
 766 Publications 297 (1), 1–17. <https://doi:10.1144/SP297.1>.
- 767 Errami, E., Bonin, B., Laduron, D., Lasri, L., 2009. Petrology and geodynamic significance of the post-  
 768 collisional Pan-African magmatism in the Eastern Saghro area (Anti-Atlas, Morocco). *J. Afr. Earth  
 769 Sci.* 55, 105–124. <https://doi:10.1016/j.jafrearsci.2009.02.006>.
- 770 Errami, E., Linnemann, U., Hofmann, M., Gärtner, A., Zieger, J., Gärtner, J., Mende, K., El Kabouri, J.,  
 771 Gasquet, D., Ennih, N., 2020. From Pan-African Transpression to Cadomian Transtension at the  
 772 West African Margin: New U–Pb zircon Ages from the Eastern Saghro Inlier (Anti-Atlas, Morocco).  
 773 *In* Murphy, J. B., Strachan, R. A. and Quesada, C. (eds). *Pannotia to Pangaea: Neoproterozoic and*  
 774 *Paleozoic Orogenic Cycles in the Circum-Atlantic Region*. Geological Society, London, Special  
 775 Publications, 503. <https://doi:10.1144/SP503-2020-105>.
- 776 Fekkak, A., Pouclet, A., Ouguir, H., Badra, L., and Gasquet, D., 1999. The Kelaat Mgouna early  
 777 Neoproterozoic Group (Saghro, Anti-Atlas, Morocco): Witness of an initial stage of the pre-Pan-  
 778 African extension: *Bulletin de la Société Géologique de France*, 170, 789–797.

- 779 Fekkak, A., Boualoul, M., Badra, L., Amenzou, M., Saquaque, A., El-Amrani, I. E., 2000. Origine et  
 780 contexte géotectonique des dépôts détritiques du Groupe Néoprotérozoïque inférieur de Kelaat  
 781 Mgouna (Anti-Atlas Oriental, Maroc). *Journal of African Earth Sciences* 30, 295–311.
- 782 Fekkak, A., Pouclet, A., Benharref, M., 2003. The Middle Neoproterozoic Sidi Flah Group (Anti-Atlas,  
 783 Morocco): synrift deposition in a Pan-African continent/ocean transition zone. *J. Afr. Earth Sci.* 37,  
 784 73–87. [https://doi:10.1016/S0899-5362\(03\)00049-6](https://doi:10.1016/S0899-5362(03)00049-6).
- 785 Ferrari, L., Lopez-Martinez, M., Rosas-Elguera, J., 2002. Ignimbrite flare-up and deformation in the  
 786 southern Sierra Madre Occidental, western Mexico: Implications for the late subduction history of  
 787 the Farallon plate. *Tectonics* 21 (4). <https://doi:10.1029/2001TC001302>.
- 788 Ferrari L, Valencia-Moreno M, Bryan S (2007) Magmatism and tectonics of the Sierra Madre  
 789 Occidental and its relation with the evolution of the western margin of North America. *Geological  
 790 Society of America Special Paper* 422: 1-39.
- 791 Folkes, C.B., de Silva, S.L., Schmitt, A.K., Cas, R.A.F., 2011. A reconnaissance of U-Pb zircon ages in  
 792 the Cerro Galán system, NW Argentina: prolonged magma residence, crystal recycling, and crustal  
 793 assimilation. *Journal of Volcanology and Geothermal Research* 206: 136–147.
- 794 Förster, H.J., Tischendorf, G., Trumbull, R.B., 1997. An evaluation of the Rb vs. (Y+ Nb) discrimination  
 795 diagram to infer tectonic setting of silicic igneous rocks. *Lithos* 40 (2), 261–293.
- 796 Frost, B.R., Barnes, C.G., Collins, W.J., Arculus, R.J., Ellis, D.J., Frost, C.D., 2001. A geochemical  
 797 classification for granitic rocks. *J. Petrol.* 42, 2033–2048.
- 798 Ganade, C.E., Lanari, P., Rubatto, D., Hermann, J., Weinberg, R.F., Basei, M.A.S., Tesser, L.R.,  
 799 Caby, R., Agbossoumonde, Y., Ribeiro, C.M., 2021. Magmatic flare-up causes crustal thickening at  
 800 the transition from subduction to continental collision. *Commun. Earth Environ.* 2 (41).
- 801 Gasquet, D., Roger, J., Chalot-Prat, F., Hassenforder, B., Baudin, T., Chèvremont, P., Razin, P.,  
 802 Benlakhdim, A., Mortaji, A., Bensaou, M., 2001. Notice explicative carte géol. Maroc (1/50 000),  
 803 feuille Tamazrar, Notes et Mémoires Serv. Géol. Maroc, n°415 bis, MEM/BRGM. Carte géologique  
 804 par Roger, J., Gasquet, D., Baudin, T., Chalot-Prat, F., Hassenforder, B., Marquer, D.,  
 805 Chèvremont, P., Berrahma, A., Destombes, J. Razin, P., Benlakhdim, M., 2001.
- 806 Gasquet, D., Levresse, G., Cheillett, A., Azizi-Samir, M.R., Mouttaqi, A., 2005. Contribution to a  
 807 geodynamic reconstruction of the Anti-Atlas (Morocco) during Pan-African times with the emphasis

- 808 on inversion tectonics and metallogenic activity at the Precambrian-Cambrian transition.
- 809 Precambrian Research 140, 157–182. <https://doi:10.1016/j.precamres.2005.06.009>.
- 810 Gasquet, D., Ennih, N., Liégeois, J-P., Soulaimani, A., Michard, A., 2008. The Panafrican belt. In:
- 811 Michard A., Saddiqi O., Chalouan A., Frizon de Lamotte D. (Eds.), Continental Evolution: The
- 812 Geology of Morocco. Structure, Stratigraphy, and Tectonics of the Africa-Atlantic-Mediterranean
- 813 Triple Junction, Springer Verl., Berlin, Heidelberg, pp. 33–64.
- 814 Geyer, G., 1990. Proposal of formal lithostratigraphical units for the Terminal Proterozoic to early
- 815 Middle Cambrian of southern Morocco. Newsl. Stratigr. 22 (2/3), 87–109.
- 816 Grunder, A.L., Klemetti, E.W., Feeley, T.C., McKee, C.M., 2008. Eleven million years of arc volcanism
- 817 at the Aucanquilcha Volcanic Cluster, northern Chilean Andes: implications for the life span and
- 818 emplacement of plutons. Transactions of the Royal Society of Edinburgh: Earth Sciences 97: 415–
- 819 436.
- 820 Hassenforder, B., 1987. La tectonique panafricaine et varisque de l'Anti-Atlas dans le massif du
- 821 Kerdous, Maroc. Thèse Doctorat ès-Sciences, Université Louis Pasteur, Strasbourg, 249 p.
- 822 Hassenforder, B., Roger, J., Baudin, T., Chalot-Prat, F., Gasquet, D., Berrahma, A., Chèvremont, P.,
- 823 Marquer, D., Razin, P., Benlakhdim, M., 2001. Carte géol. Maroc (1/50 000), feuille Sidi Bou'addi.
- 824 Notes et Mémoires Serv. Géol. Maroc, n°414.
- 825 Hawkins, M.P., Beddoe-Stephens, B., Gillespie, M.R., Loughlin, S., Barron, H.F., Barnes, R.P., Powell,
- 826 J.H., Waters, C.N., Williams, M., 2001. Carte géologique du Maroc au 1/50 000, feuille Tiwit. Notes
- 827 et Mémoires du Service Géologique du Maroc 404.
- 828 Hefferan, K., Soulaimani, A., Samson, S.D., Admou, H., Inglis, J., Saquaque, A., Latifa, C., Heywood,
- 829 N., 2014. A reconsideration of Pan African orogenic cycle in the Anti-Atlas Mountains, Morocco. J.
- 830 Afr. Earth Sci. 98, 34–46. <https://doi.org/10.1016/j.jafrearsci.2014.03.007>
- 831 Hildebrand, R.S., Whalen, J.B., 2014. Arc and slab-failure magmatism in Cordilleran batholiths II – The
- 832 Cretaceous Peninsular Ranges Batholith of southern and Baja California. Geoscience Canada, 41,
- 833 399–458. <https://doi.org/10.12789/geocanj.2014.41.059>
- 834 Hildebrand, R.S., Whalen, J.B., 2017. The tectonic setting and origin of Cretaceous batholiths within
- 835 the North American Cordillera: The case for slab failure magmatism and its significance for crustal
- 836 growth. Geological Society of America Special Paper 532, 113 p. <https://doi:10.1130/2017.2532>.

- 837 Hildebrand, R.S., Whalen, J.B. and Bowring, S.A. 2018. Resolving the crustal composition paradox by  
 838 3.8 billion years of slab failure magmatism and collisional recycling of continental crust.  
 839 *Tectonophysics*, 734–735, 69–88. <https://doi.org/10.1016/j.tecto.2018.04.001>
- 840 Hollard, H., Choubert, G., Bronner, G., Marchand, J., Sougy, J., 1985. Carte géologique du Maroc,  
 841 échelle: 1/1.000.000. Notes Mém. Serv. Géol. Maroc, n°260.
- 842 Ikenne, M., Soderlund, U., Ernst, R., Pin, C., Youbi, N., El Aouli, E.H., 2017. A c. 1710 Ma mafic sill  
 843 emplaced into a quartzite and calcareous series from Igherm, Anti-Atlas, Morocco: evidence that  
 844 the Taghdout passive margin sedimentary group is nearly 1 Ga older than previously thought. *J.*  
 845 *Afr. Earth Sci.* 127, 113–135. <https://doi:10.1016/j.jafrearsci.2016.08.020>.
- 846 Inglis, J.D., MacLean, J.S., Samson, S.D., D'Lemos, R.S., Admou, H., Hefferan, K., 2004. A precise U-  
 847 Pb zircon age for the Bleïda granodiorite, Anti-Atlas, Morocco: implications for the timing of  
 848 deformation and terrane assembly in the eastern Anti-Atlas. *J. Afr. Earth Sci.* 39, 277–283.  
 849 <https://doi:10.1016/j.jafrearsci.2004.07.041>.
- 850 Karaoui, B., Breitkreuz, C., Mahmoudi, A., Youbi, N., 2014. Physical volcanology, geochemistry and  
 851 basin evolution of the Ediacaran volcano-sedimentary succession in the Bas Draâ inlier  
 852 (Ouarzazate Supergroup, Wtesern Anti-Atlas, Morocco. *J. Afr. Earth Sci.* 99, 307–331.  
 853 <https://doi:10.1016/j.jafrearsci.2014.06.022>.
- 854 Karaoui, B., Breitkreuz, C., Mahmoudi, A., Youbi, N., Hofmann, M., Gärtner, A., Linnemann, U., 2015.  
 855 U-Pb ages from volcanic and sedimentary rocks of the Ediacaran Bas Draâ inlier (Anti-Atlas  
 856 Morocco): Chronostratigraphic and provenance implications. *Precambrian Res.* 263, 43–58.  
 857 <https://doi:10.1016/j.precamres.2015.03.003>.
- 858 Kouyaté, D., Söderlund, U., Youbin N., Ernst, R., Hafid, A., Ikenne, M., Soulaimani, A., Bertrand, H., El  
 859 Janati, M., R'kha Chaham, K., 2013. U-Pb baddeleyite and zircon ages of 2040 Ma, 1650 Ma and  
 860 885 Ma on dolerites in the West African Craton (Anti-Atlas inliers): Possible links to break-up of  
 861 Precambrian supercontinents. *Lithos* 174, 71–84. <https://doi:10.1016/j.lithos.2012.04.028>.
- 862 Leblanc, M., 1975. Ophiolites précambriennes et gîtes arseniés de cobalt (Bou Azzer - Maroc). Ph.D.  
 863 Dissertation. Paris, France, Université de Paris VI, 329 pp.
- 864 Lipman, P.W., Prostka, H.J., Christiansen, R.L., 1971. Evolving subduction zones in the western  
 865 United States, as interpreted from igneous rocks. *Science* 174, 821–825.

- 866 Pelleter, E., Cheilletz, A., Gasquet, D., Mouttaqi, A., Annich, M., El Hakour, A., Deloule, E., Féraud, G.,  
 867 2007. Hydrothermal Zircons: A tool for ion microprobe U-Pb dating of gold mineralization (Tamlalt-  
 868 Menhouhou Gold deposit - Morocco). *Chemical Geology* 245: 135–161.
- 869 Lima, S.M., Corfu, F., Neiva, A.M.R., Ramos, J.M.F., 2012. Dissecting complex magmatic processes:  
 870 an in-depth U-Pb study of the Pavia Pluton, Ossa-Morena Zone, Portugal. *Journal of Petrology* 53:  
 871 1887–1911.
- 872 Lipman, P.W., Prostka, H.J., Christiansen, R.L., 1972. Cenozoic volcanism and plate-tectonic  
 873 evolution of the western United States. I. Early and Middle Cenozoic. *Philosophical Transactions of  
 874 the Royal Society of London A* 271: 217–248.
- 875 Maacha, L., Azizi-Samir, M.-R., Bouchta, R., 1998. Gisements cobaltifères du district de Bou Azzer  
 876 (Anti-Atlas). Structure, minéralogie et conditions de genèse. *Chron. Rech. Minière*, 531-532, 65–  
 877 75.
- 878 Manea, V.C., Leeman, W.P., Gerya, T., Manea, M., Zhu, G., 2014. Subduction of fracture zones  
 879 controls mantle melting and geochemical signature above slabs. *Nat. Commun.* 5, 1–10.
- 880 Michard, A., Soulaimani, A., Ouanaïmi, H., Raddi, Y., Ait Brahim, L., Rjimati, E., Baïdder, L., Saddiqi,  
 881 O., 2017. Saghro Group in the Ougnat Massif (Morocco), an evidence for a continuous Cadomian  
 882 basin along the northern West African Craton. *C. R. Geoscience* 349, 81–90.  
 883 <https://doi:10.1016/j.crte.2017.01.001>.
- 884 Mortaji A., Ikenne M., Gasquet D., Barbey P., Stussi J. M., 2000. Les granitoïdes paléoprotérozoïques  
 885 des boutonnières du Bas Drâa et de la Tagraga d'Akka (Anti-Atlas occidental, Maroc) : un élément  
 886 du puzzle géodynamique du craton ouest- africain. *J. African. Earth Sci.*, 31: 523–538.  
 887 [https://doi:10.1016/S0899-5362\(00\)80005-6](https://doi:10.1016/S0899-5362(00)80005-6).
- 888 Mrini Z., 1993. Chronologie (Rb-Sr, U-Pb), traçage isotopique (Sr-Nd-Pb) des sources des roches  
 889 magmatiques éburnéennes, panafricaines et hercyniennes du Maroc. Thèse Doctorat es Sciences,  
 890 Université Cadi Ayad, Marrakech, 227 p.
- 891 Noble, D.C., 1972. Some observations on the Cenozoic volcano-tectonic evolution of the Great Basin,  
 892 western United States. *Earth Planet. Sci. Lett.* 17, 142–150.
- 893 O'Connor, E.A., 2010. Geology of the Draâ, Kerdous, and Boumalne Districts, Anti-Atlas, Morocco.  
 894 Technical Report IR/10/072, British Geological Survey, Keyworth, Nottingham, England.

- 895 Ouguir, H., Macaudiere, J., Dagallier, G., 1996. Le protérozoïque supérieur d'imiter, Saghro oriental,  
 896 Maroc: un contexte géodynamique d'arrière-arc. *Journal of African Earth Sciences* 22, 173–189.  
 897 [https://doi:10.1016/0899-5362\(96\)00002-4](https://doi:10.1016/0899-5362(96)00002-4).
- 898 Piqué, A., 2003. Evidence for an important extensional event during the latest proterozoic and earliest  
 899 paleozoic in morocco. *C. R. Geosci.* 335, 865–868.
- 900 Piqué, A., Bouabdelli, M., Soulaimani, A., Youbi, N., Iliani, M., 1999. The Late Proterozoic III  
 901 conglomerates of the Anti-Atlas (southern Morocco). Their relationships with the Panafrican  
 902 orogeny or a Late Proterozoic rifting episode. *Comptes Rendus de l'Académie des Sciences* 328,  
 903 409–414. [https://doi:10.1016/S1251-8050\(99\)80107-4](https://doi:10.1016/S1251-8050(99)80107-4).
- 904 Roger, J., Gasquet, D., Baudin, T., Chalot-Prat, F., Hassenforder, B., Marquer, D., Chèvremont, P.,  
 905 Berrahma, A., Destombes, J. Razin, P., Benlakhdim, M., 2001. Carte géol. Maroc (1/50 000), feuille  
 906 Tamazrar. *Notes et Mémoires Serv. Géol. Maroc*, n°415.
- 907 Roger, J., Chèvremont, P., Razin, P., Thiéblemont, D., Baudin, T., Calvès, G., Anzar-Conseil, 2005.  
 908 Notice explicative, carte géol. Maroc (1/50 000), feuille Tlatat Ida Gougmar, *Notes et Mém. Serv.*  
 909 *Géol. Maroc*, n°498bis, MEM/BRGM, 105 p. Carte géol. par Calvès G., Gabudianu D., Chèvremont  
 910 P., Roger J., Razin P., (2005), *Notes et Mém. Serv. Géol. Maroc*, n°498.
- 911 Saquaque, A., Benharref, M., Abia, H., Mrini, Z., Reuber, I., Karson, J. A., 1992. Evidence for a  
 912 Panafrican volcanic arc and wrench fault tectonics in the Jbel Saghro, Anti-Atlas, Morocco.  
 913 *Geologische Rundschau* 81, 1–13.
- 914 Schwartz, J.J., Klepeis, K.A., Sadorski, J.F., Stowell, H.H., Tulloch, A.J., Coble, M.A., 2017. The  
 915 tempo of continental arc construction in the Mesozoic Median Batholith, Fiordland, New Zealand.  
 916 *Lithosphere* 9, 343–365.
- 917 Skilling, I.P., 1994. Evolution of an englacial volcano: Brown Bluff, Antarctica. *Bull Volcanol* 56, 573–  
 918 591.
- 919 Smellie, J.L., Skilling, I.P., 1994. Products of subglacial volcanic eruptions under different ice  
 920 thickness: two examples from Antarctica. *Sedimentary Geology* 91, 115–129.
- 921 Soulaimani, A., Bouabdelli, M., Piqué, A., 2003. L'extension continentale au Néoprotérozoïque  
 922 supérieur – Cambrien inférieur dans l'Anti-Atlas (Maroc). *Bull. de la Société Géologique de France*  
 923 174, 83–92. <https://doi:10.2113/174.1.83>

- 924 Soulaimani, A., Essaifi, A., Youbi, N., Hafid, A., 2004. Les marqueurs structuraux et magmatiques de  
 925 l'extension crustale au Protérozoïque terminal-Cambrien basal autour du massif de Kerdous (Anti-  
 926 Atlas occidental, Maroc). *C. R. Geoscience* 336, 1433–1441. <https://doi:10.1016/j.carte.2004.03.020>
- 927 Soulaimani, A., Blein, O., Chèvremont, Ph., Ouainami, H., Hafid, A., Admou, H., Baudin, T.,  
 928 Bouabdelli, M., Razin, Ph., Abia, E.H., Beni Akhy, R., 2013. Notice explicative carte géol. Maroc  
 929 (1/50 000), feuille Agadir Melloul, Notes et Mémoires Serv. Géol. Maroc, n°549, MEM/BRGM.  
 930 Carte géologique par Blein, O., Roger, J., Chèvremont, Ph., Baudin, T., Soulaimani, A., Ouainami,  
 931 H., Admou, H., Hafid, A., Abia, E.H., Bouabdelli, M., 2013.
- 932 Soulaimani, A., Ouainami, H., Michard, A., Monterod, P., Bead, F., Corsini, M., Molinad, J.-F., Rjimati,  
 933 E.-C., Saddiqig, O., Hefferan, K., 2019. Quartzite crests in Paleoproterozoic granites (Anti-Atlas,  
 934 Morocco); a hint to Pan-African deformation of the West African Craton margin. *J. Afr. Earth Sci.*  
 935 2019; 157(February):103501. <https://doi:10.1016/j.jafrearsci.2019.05.009>.
- 936 Sun, S.S., McDonough, W.F., 1989. Chemical and isotopic systematics of oceanic basalts:  
 937 implications for mantle composition and processes. In: Saunders, A.D., Norry, M.J. (Eds.),  
 938 *Magmatism in the Ocean Basins*, 42 (Special publication). Geological Society, 313–345.
- 939 Thomas, R.J., Chevallier, L.C., Gresse, P.G., Harmer, R.E., Eglington, B.M., Armstrong, R.A., de  
 940 Beer, C.H., Martini, J.E.J., de Kock, G.S., Macey, P., Ingram, B., 2002. Precambrian evolution of  
 941 the Siroua Window, Anti-Atlas Orogen, Morocco. *Precambrian Research* 118, 1–57.  
 942 [https://doi:10.1016/S0301-9268\(02\)00075-X](https://doi:10.1016/S0301-9268(02)00075-X).
- 943 Thomas, R.J., Fekkak, A., Errami, E., Loughlin, S.C., Gresse, P.G., Chevallier, L.P., Liégeois, J.-P.,  
 944 2004. A new lithostratigraphic framework for the Anti-Atlas Orogen, Morocco. *Journal of African*  
 945 *Earth Sciences*, 39, pp. 217–226. <https://doi:10.1016/j.jafrearsci.2004.07.046>.
- 946 Toummite, A., Liégeois, J.-P., Gasquet, D., Bruguier, O., Beraaouz, E.H., Ikenne, M., 2012. Field,  
 947 geochemistry and Sr-Nd isotopes of the Pan- African granitoids from the Tifnoute Valley (Sirwa,  
 948 Anti-Atlas, Morocco): a post-collisional event in a metacratonic setting. *Mineral. Petrol.* 107 (5),  
 949 739–763. <https://doi:10.1007/s00710-012-0245-3>.
- 950 Tuduri, J., Chauvet, A., Barbanson, L., Bourdier, J.L., Labriki., M., Ennaciri, A., Badra, L., Dubois, M.,  
 951 Ennaciri-Leloix, C., Sizaret, S., Maacha, L., 2018. The Jbel Saghro Au(-Ag, Cu) and Ag-Ah  
 952 metallogenetic province: Product of a long-lived Ediacaran tectono-magmatic evolution in the  
 953 Moroccan Anti-Atlas. *Minerals* 8, 592. <https://doi:10.3390/min8120592>.

- 954 Walsh, G.E., Aleinikoff, J.N., Benziane, F., Yazidi, A., Armstrong, T.R., 2002. U-Pb zircon  
 955 geochronology of the Paleoproterozoic Tagagra de Tata inlier and its Neoproterozoic cover,  
 956 western Anti-Atlas, Morocco. *Precambrian Research* 117, 1–20. [https://doi:10.1016/S0301-9268\(02\)00044-X](https://doi:10.1016/S0301-9268(02)00044-X)
- 957
- 958 Walsh, G.J., Benziane, F., Aleinikoff, J.N., Harisson, R.W., Yazidi, A., Burton, W.C., Quick, J.E.,  
 959 Saadane, A., 2012. Neoproterozoic tectonic evolution of the Jebel Saghro and Bou Azer-El Graara  
 960 inliers, eastern and central Anti-Atlas, Morocco. *Precambrian Res.* 216-219, 23–62.  
 961 <https://doi:10.1016/j.precamres.2012.06.010>.
- 962 Whalen, J.B., Hildebrand, R.S., 2019. Trace element discrimination of arc, slab failure, and A-type  
 963 granitic rocks. *Lithos* 248-349, 105179. <https://doi:10.1016/j.lithos.2019.105179>.
- 964 Yajoui Z., Karaoui, B., Chew, D., Breitkreuz, C., Mahmoudi, A., 2020. U-Pb zircon geochronology of  
 965 the Ediacaran volcano-sedimentary succession of the NE Saghro inlier (Anti-Atlas, Morocco):  
 966 Chronostratigraphic correlation on the northwestern margin of Gondwana. *Gondwana Res.*, 87,  
 967 263-277. <https://doi:10.1016/j.gr.2020.06.015>.
- 968 Youbi, N., 1998. Le volcanisme « post-collisionnel »: un magmatisme intraplaque relié à des panaches  
 969 mantelliques. Etude volcanologique et géochimique. Exemples d'application dans le  
 970 Néoprotérozoïque terminal (P III) de l'Anti-Atlas et le Permien du Maroc. (PhD thesis). Université de  
 971 Marrakech
- 972 Youbi, N., Kouyaté, D., Söderlund, U., Ernst, R.E., Soulaimani, A., Hafid, A., Ikenne, M., El Bahat, A.,  
 973 Bertrand, H., Rkha Chaham, K., Ben Abbou, M., Mortaji, A., El Ghorfi, M., Zouhair, M., El Janati,  
 974 M., 2013. The 1750 Ma magmatic event of the West African Craton (Anti-Atlas), Morocco.  
 975 *Precambrian Res.* 236, 106–123. <https://doi:10.1016/j.precamres.2013.07.003>.

976 **Tables**977 **Table 1:** Variation contents of REEs in the Tagragra-n-Daouizid rhyolites.978 **Table S1:** Representative chemical analyses of volcanic rocks from Tagragra Ouhallal.979 **Table S2:** Representative chemical analyses of volcanic rocks from Tagragra-n-Daouizid.980 **Table S3:** Representative chemical analyses of volcanic rocks from south Kerdous inlier.

|                      | Tagraga-n-Daouizid rhyolites |           |                |                |
|----------------------|------------------------------|-----------|----------------|----------------|
|                      | Group I                      | Group II  | Group III      | Group IV       |
| [La/Yb] <sub>n</sub> | 20 - 60                      | 25 - 36   | 8 - 17         | 1.5 - 22       |
| [Yb] <sub>n</sub>    | <5                           | <10       | >10            | <10            |
| [La/Sm] <sub>n</sub> | 2.7 - 8.9                    | 4.4 - 5.0 | 3.0 - 4.1      | 2.3 - 4.1      |
| [Gd/Yb] <sub>n</sub> | 2.8 - 8.3                    | 2.8 - 4.5 | 1.6 - 3.0      | 0.9 - 2.9      |
| Eu anomalie          | negative                     | no        | light negative | light negative |
| $\Sigma$ REE ppm     | 75 - 200                     | 165 -210  | 185 -300       | 35 -55         |

## Highlights

- An Upper Ediacaran felsic pyroclastic magmatism, the Ouarzazate Group
- Felsic rocks generated by partial melting of crustal lithologies.
- Rare mafic rocks evolve from calc-alkaline to continental tholeiitic affinities.
- Few intermediate and felsic rocks characteristics of slab failure context.

**Declaration of competing interest**

The authors declare that they have no known competing financial interests or personal relationships that could have appeared to influence the work reported in this paper.